NASA/TM-2008-215308

Characterization of Fatigue Damage for Bonded Composite Skin/Stringer Configurations

Isabelle Paris and Michael Cvitkovich
National Research Council
Langley Research Center, Hampton, Virginia

Ronald Krueger
National Institute of Aerospace, Hampton, Virginia

May 2008

The NASA STI Program Office . . . in Profile

Since its founding, NASA has been dedicated to the advancement of aeronautics and space science. The NASA Scientific and Technical Information (STI) Program Office plays a key part in helping NASA maintain this important role.

The NASA STI Program Office is operated by Langley Research Center, the lead center for NASA's scientific and technical information. The NASA STI Program Office provides access to the NASA STI Database, the largest collection of aeronautical and space science STI in the world. The Program Office is also NASA's institutional mechanism for disseminating the results of its research and development activities. These results are published by NASA in the NASA STI Report Series, which includes the following report types:

- TECHNICAL PUBLICATION. Reports of completed research or a major significant phase of research that present the results of NASA programs and include extensive data or theoretical analysis. Includes compilations of significant scientific and technical data and information deemed to be of continuing reference value. NASA counterpart of peer-reviewed formal professional papers, but having less stringent limitations on manuscript length and extent of graphic presentations.

- TECHNICAL MEMORANDUM. Scientific and technical findings that are preliminary or of specialized interest, e.g., quick release reports, working papers, and bibliographies that contain minimal annotation. Does not contain extensive analysis.

- CONTRACTOR REPORT. Scientific and technical findings by NASA-sponsored contractors and grantees.

- CONFERENCE PUBLICATION. Collected papers from scientific and technical conferences, symposia, seminars, or other meetings sponsored or co-sponsored by NASA.

- SPECIAL PUBLICATION. Scientific, technical, or historical information from NASA programs, projects, and missions, often concerned with subjects having substantial public interest.

- TECHNICAL TRANSLATION. English-language translations of foreign scientific and technical material pertinent to NASA's mission.

Specialized services that complement the STI Program Office's diverse offerings include creating custom thesauri, building customized databases, organizing and publishing research results ... even providing videos.

For more information about the NASA STI Program Office, see the following:

- Access the NASA STI Program Home Page at ***http://www.sti.nasa.gov***

- E-mail your question via the Internet to help@sti.nasa.gov

- Fax your question to the NASA STI Help Desk at (301) 621-0134

- Phone the NASA STI Help Desk at (301) 621-0390

- Write to:
  NASA STI Help Desk
  NASA Center for AeroSpace Information
  7115 Standard Drive
  Hanover, MD 21076-1320

NASA/TM-2008-215308

Characterization of Fatigue Damage for Bonded Composite Skin/Stringer Configurations

Isabelle Paris and Michael Cvitkovich
National Research Council
Langley Research Center, Hampton, Virginia

Ronald Krueger
National Institute of Aerospace, Hampton, Virginia

National Aeronautics and
Space Administration

Langley Research Center
Hampton, Virginia 23681-2199

May 2008

Available from:

NASA Center for AeroSpace Information (CASI)
7115 Standard Drive
Hanover, MD 21076-1320
(301) 621-0390

National Technical Information Service (NTIS)
5285 Port Royal Road
Springfield, VA 22161-2171
(703) 605-6000

Characterization of Fatigue Damage for Bonded Composite Skin/Stringer Configurations

Isabelle Paris[1], Michael Cvitkovich[2]
National Research Council, NASA Langley Research Center, Hampton, Virginia

Ronald Krueger
National Institute of Aerospace, Hampton, Virginia

ABSTRACT

The fatigue damage was characterized in specimens which consisted of a tapered composite flange, representing a stringer or frame, bonded onto a composite skin. Quasi-static tension tests were performed first to determine the failure load. Subsequently, tension fatigue tests were performed at 40%, 50%, 60% and 70% of the failure load to evaluate the debonding mechanisms between the skin and the bonded stringer. For four specimens, the cycling loading was stopped at intervals and the specimens were taken out of the grips. Photographs of the polished specimen edges were taken under a light microscope to document the occurrence and growth of matrix crack and delaminations. At two diagonally opposite corners of the flange, a delamination appeared to initiate at the flange tip from a matrix crack in the top 45° skin ply and propagated at the top 45°/-45° skin ply interface. At the other two diagonally opposite corners, a delamination running in the bondline initiated from a matrix crack in the adhesive pocket. Dye penetrant X-ray radiography was also used to measure the amount of delamination through the width. In addition, two specimens were cut longitudinally into several sections. Photographs of the polished section edges were taken under a light microscope to document the damage inside the specimens. These micrographs reveal a more complex pattern inside the specimen where the two delamination patterns observed at the edges are present simultaneously across most of the width of the specimen. The observations suggest that a more sophisticated nondestructive evaluation technique such as a D-scan, time-of-flight scan or depth scan is required to capture the complex damage pattern of matrix cracking and multi-level delaminations. With respect to finite element modeling of delaminations and predicting their propagation and growth, the question arises of how much simplification is permissible and how much detail is required in order to properly capture the damage mechanism.

[1] Current affiliation: Composites Innovations Inc., Montreal, Canada.

[2] Current affiliation: Daimler AG, Wörth, Germany.

INTRODUCTION

Many composite components in aerospace structures are made of flat or curved panels with co-cured or adhesively bonded frames and stiffeners. Testing of skin gage stiffened panels designed for pressurized aircraft fuselages has shown that bond failure at the tip of the frame flange is an important and very likely failure mode [1]. The same type of skin-stiffener debonding failure is observed when a thin-gage composite fuselage structure is allowed to buckle. Comparatively simple specimens consisting of a stringer flange bonded onto a skin have been developed to study skin/stiffener debonding [2-4]. The failure that initiates at the tip of the flange in these specimens is nearly identical to the failure observed in the full-scale panels and the frame pull-off specimens [3, 5]. To obtain a more complete understanding of skin/stringer debonding mechanisms, it is vital to perform fatigue tests along with the monotonic experiments to establish the durability of these bonded joints over the anticipated life cycle. Four-point bending fatigue tests were carried out in a previous study [6].

The objective of this work was to study the damage mechanisms in bonded composite skin/stringer structures under tension fatigue loading conditions. The specimens consisted of a tapered flange, representing the stringer bonded onto a skin. In a related study, static tension tests had been performed to evaluate the debonding mechanisms between the skin and the bonded flange and yield static failure loads. Then, tension fatigue tests were performed at load levels corresponding to 40%, 50%, 60%, and 70% of the damage onset loads. Microscopic investigations of the specimen edges and X-ray photography were used to document the onset of matrix cracking and delamination as a function of fatigue cycles. The results were used to develop a methodology for cumulative life prediction of bonded composite skin/stringer structures based on delamination fatigue characterization data and geometrically nonlinear finite element analyses [7]. The two- and three-dimensional analyses accounted for different locations where the first delamination might occur, however, they were based on the assumption that there was only one plane of delamination across the entire width of the specimen [8] [9].

The intent of the current work was to identify the typical damage patterns observed in the specimen and to summarize and document the experimental work. First, the specimens and the experimental procedure are described, and the results of the static tests are summarized. Second, the results of the tension fatigue tests which were performed at load levels corresponding to 40%, 50%, 60%, and 70% of the damage onset loads are summarized. Third, the typical damage patterns in the specimens are identified, which is the focus of the current work. For four specimens, the cycling loading was stopped at intervals, and the specimens were taken out of the grips. Photographs of the polished specimen edges were taken under a light microscope to document the occurrence and growth of matrix cracks and delaminations. Additionally, dye penetrant X-ray radiography was used to measure the amount of delamination across the width. In addition, two specimens were cut longitudinally into four and seven sections, respectively. Photographs of the polished section edges were taken under a light microscope to document the matrix cracks and delaminations and thus identify the typical damage pattern.

MATERIALS AND SPECIMEN PREPARATION

The specimens consisted of a tapered flange, representing the stringer, bonded onto a skin (Figure 1a). An IM7/8552 graphite/epoxy system manufactured by Hexcel Corporation was used for the skin and flange. The skin lay-up for panels 3 and 6 was [45/-45/0/-45/45/90/90/-45/45/0/45/-45] using prepreg tape. The flange was made of a plain-weave fabric, and the lay-up was $[45/0/45/0/45/0/45/0/45]_f$ where 0 represents a 0°-90° fabric ply and 45 represents a 0°-90° fabric ply rotated 45°.

For panel 2, the orientation of one layer was incorrect, resulting in the following skin lay-up: [45/-45/0/-45/45/90/90/0/45/0/45/-45]. These specimens were also tested. The layup of each specimen is documented in Table I. For panels 4 and 5, the orientation of the layers was rotated, resulting in the following skin lay-up: [-45/45/90/45/-45/0/0/45/-45/90/-45/45]. In order to be able to compare results for the different load levels and obtain a fatigue life curve, it was decided to exclude the specimens with the rotated lay-up from the test matrix of the fatigue testing and focus on the specimens cut from panels 3 and 6.

The flange was pre-cured, cut to size, machined with a 25° taper along the edges and co-bonded with the uncured skin using one ply of grade 5, FM® 300 film adhesive manufactured by Cytec Engineered Materials. The averaged ply thickness obtained from specimen thickness measurements and micrographs was 0.148 mm for the tape, 0.212 mm for the fabric and 0.178 mm for the adhesive.

EXPERIMENTAL PROCEDURE

Quasi-static

Quasi-static tension tests were performed in a servohydraulic load frame in displacement control at 0.4 mm/min. The specimens were mounted in hydraulic grips with a gage length of 101.6 mm. A total of five specimens was tested. Two specimens were equipped with two strain gages, one located in the center of the flange and the other located on the skin as close to the flange tip as possible (see Figure 1a). The remaining three specimens had the gage on the flange only. In addition to the strain gages, an extensometer with a 25.4 mm gage length was mounted on the backside of the specimens and centered on the flange tip as displayed in Figure 1b. The tests were terminated when the flange debonded from the skin.

Fatigue tests

The fatigue test configuration is the same as the one used for the quasi-static tests. Fatigue tests were performed at a cyclic frequency of 5 Hz, an R-ratio of 0.1 and load levels corresponding to 40%, 50%, 60% and 70% of the quasi-static damage onset load. Four tests were performed at 40% and 60% and three tests were performed at 50% and 70% as documented in Table I. During the test, the damage was monitored in-situ using a *Questar®* digital microscope manufactured by Company Seven, Astro-Optics Division. The digital microscope was used on one edge and an optical travelling microscope on the other edge as shown in the test set-up in Figure 2a. The specimen edges were painted white to make the cracks and delaminations more visible as shown in Figure 2b. Damage

was documented based on location at each of the four corners identified in Figure 1a. The number of cycles at which the first matrix crack appeared was recorded as well as the number of cycles to delamination onset. After the test, the specimen was clamped into a three-point bending rig shown in Figure 3a. A small load was applied by hand tightening a set screw to open the matrix crack and delamination and therefore increase the visibility of the damage as shown in Figure 3b. A photograph of the polished specimen edge was then taken under a light microscope as shown in Figure 3c.

3-D mapping of the damage

For four specimens (9B-02, 7B-06, 8B-06 and 10B-03), the cycling loading was interrupted several times. During the interruption, the specimen was taken out of the grips. Using the same bending rig described previously, a photograph of the polished specimen edge was then taken under a light microscope to document the occurrence and growth of matrix cracks and delaminations. The specimen was then returned to the loading frame and the cyclic loading continued.

Furthermore, dye penetrant X-ray radiography was used to measure the amount of delamination across the width. Zinc-iodide based X-ray dye penetrant was deposited on the specimen edges and flange tip and allowed to soak into the specimen for a minimum of 15 minutes. Radiographs of the specimen were then recorded on *type 53 coaterless 4"x5" instant black and white film* manufactured by *Polaroid®*. The area of interest and the corresponding enhanced image are shown in Figure 4. One difficulty encountered is that the delamination occurs right below the bevel of the flange. The change in specimen thickness will result in a change of gray levels in that zone, rendering the delamination difficult to detect. This difficulty was solved by taking an X-ray image before testing (see Figure 5a) and using a digital image processing technique to subtract the undamaged specimen image from the damaged specimen image (see Figure 5b). The images were digitized using a flatbed scanner. A resolution of 600 dots per inch was used. The image processing was done using the software *Photoimpact®* manufactured by *Ulead* and consisted of the following steps: the images were first rotated by aligning vertically the left edge of the specimen, then the undamaged specimen image was inverted. Then, the "stiching" function with a degree of transparency of 50% was used to align the two images on top of each other and combine them. The resulting enhanced image is shown in Figure 5c. Care had to be taken when taking the X-ray image radiograph to obtain an appropriate brightness and contrast, constant from image to image. To align the images, the strain gauge was used if present, or a piece of aluminum tape was placed on the specimen prior to taking the X-ray image.

Finally, two specimens (8B-06 and 10B-03) were cut longitudinally in several slices as shown in the drawings of Figure 6 and the photographs in Figure 7. The thicknesses w_i of the i slices as well as the distance z_{ir} and z_{il} to the right and left edges of the slices (measured from the left edge of the specimen) are documented in Table I. The edges of each slice were polished (marked with a red star) and photographed under a light microscope, as described before. The measurement of the delamination length was combined with information about the location of the delamination through the thickness to obtain a 3-D mapping of the damage as discussed later.

TESTS RESULTS

Quasi-static tests

In Figures 8 and 9, typical results are shown as plots of load versus displacement and strain versus load, respectively. The loads, flange and skin strains are reported in Table II for the point of possible damage initiation as well as for the maximum sustained load. For the specimens with two strain gages (2B02 and 2B03), the strain values are shown for flange strain and skin strain, respectively. For the remaining specimens, these values are shown for flange strain only.

The load-displacement curves were slightly nonlinear over a wide range as shown in Figure 8. Possible damage initiation was assumed when a small initial load drop was observed prior to flange debonding. At this point, a crack in one flange tip or a small delamination along one flange corner was observed. In two specimens (2B02 and 6B06), no initial load drop or visible damage could be detected. In general, the initial load drop occurred above 90% of the maximum sustained load. The nonlinear strain-load response up to flange debonding is shown in Figure 9. Initially, flange strains dropped before rising again with increasing load. The initial compression phase captured by the strain gage is caused by secondary bending due to the load eccentricity in the flange region and the asymmetric layup with respect to the neutral axis. In all specimens, a load drop was also accompanied by a decrease in strain. The same three specimens that showed a load drop in the load-displacement plots also displayed a drop in flange strain prior to flange debonding. Skin strains were nearly linear until flange debonding occurred, as shown in Figure 9. The value of the damage onset load was averaged from five tests and determined to be 17.8 kN which was later designated as $P_{100\%}$.

Fatigue tests

The load level as a function of the number of cycles to matrix crack onset is shown in Figure 10 for the specimens made from panels 3 and 6 (red squares). The loads at onset of damage obtained from the quasi-static tests are shown on the ordinate (green circles). These data points represent the damage initiation loads given in Table II. The mean values for each load level are represented by solid symbols. The load level as a function of the number of cycles to delamination onset is shown in Figure 11 for the specimens made from panels 3 and 6 (purple diamonds). The number of cycles to delamination onset is a cumulative number and includes the cycles to matrix crack onset. There is a considerable difference between matrix crack onset and delamination onset, especially when considering the mean values. An almost linear relationship between P_{max} and log N can be also observed for delamination onset, with some scatter between the replicates tested at each load levels [7]. The results obtained from specimens made from panel 2 were added to the plots as shown in Figure 12 and 13. The specimens made from panel 2 exhibit a longer life compared to the life of the specimens made from panels 3 and 6. This is to be expected, since the lay-up of panel 2 leads to a stiffer specimen resulting in a lower stress at the flange tip.

MICROSCOPIC INVESTIGATION

Typical damage patterns observed at the flange tip are shown in Figures 14 and 15. Two typical micrographs were included. All quasi-static and fatigue tests yielded similar damage patterns. Under quasi-static loading, failure occurred across one flange tip of the specimen only, with no clear preference for corners 1 and 2 or corners 3 and 4 shown in Figure 1. In fatigue, damage initiated at both flange tips, but not at the same time.

At corners 2 and 3, a delamination (B, in blue) formed in the top 45°/-45° skin ply interface, as depicted in Figure 14. For the quasi-static case, the damage can only be observed after the test, and it appears that this delamination initiated at the flange tip from a matrix crack in the top 45° skin ply as shown in Figure 14(a,b). In fatigue, the sequence of events, as depicted in Figure 14(c), has been observed with a *Questar®* microscope. The first matrix crack occurs in the adhesive pocket (①), then grows through the top 45° skin ply and forms a delamination B (② in violet) in the top 45°/-45° skin ply interface growing towards the center of the flange (①→②). Sometimes, the delamination B (③, in blue) grows back towards the grip and causes a matrix crack through the top 45° ply, reaching the skin surface (③→④). The original matrix crack through the adhesive pocket and top 45° ply closes (①). The closure explains the observations from the static case, where the matrix crack through the adhesive pocket was not observed (see Figure 14(a)).

At corners 1 and 4, a delamination running in the bondline (A1, in green) initiated from a matrix crack in the adhesive pocket, as shown in Figure 15. In some of the quasi-static cases, a second delamination (A2, in orange) was observed below the first one, in the top –45°/0° skin ply interface. Delamination A2 was not observed in fatigue presumably, because the load levels were lower compared to the static test.

In fatigue, damage first appeared at corner 2 and 3 (delamination B) for 12 of the 14 specimens. The delamination lengths were measured using the traveling stage of the optical microscope while the edges were still covered with white paint. The lengths measured for four specimens (9B-02, 7B-06, 8B-06 and 10B-03) after different numbers of load cycles are listed in Table III. The mechanics are discussed in the section on the mechanics of failure.

3-D DAMAGE MAPPING

Images obtained form X-ray radiography

The final images obtained from X-ray radiography and image post-processing are shown in Figures 16 to 19 for four specimens (9B-02, 7B-06, 8B-06 and 10B-03) after different load cycles. The dark areas where the contrast fluid had penetrated into the damaged section of the specimen reveal the delaminations. In the image of Figure 16(a) - taken from specimen 8B-06 after 279 cycles, a delamination was only visible along the flange edge from corners 3 to 4. The gray intensity appeared to be more pronounced towards corner 3 (delamination B), which suggests an increased growth in this area. This observation is confirmed by Figure 16(b) (taken after 506 cycles) and Figure 16(c) (taken after 730 cycles) where the delamination appears the have grown further to corner 3 (delamination B). Delamination growth at the opposite flange edge (from corner 1 to 2) was also observed as shown in Figures 16(b) and (c). The growth appeared to be slower

and more uniform compared to the other edge. The observations were verified by cutting the specimens into slices as shown in Figures 6 and 7. Micrographs of the edges were obtained to reveal the growth in the interior of the specimen. The observations are discussed later.

The images for the other specimens (10B-03, 9B-02 and 7B-06) reveal a similar growth pattern as shown in Figures 17, 18 and 19. For specimen 10B-03, shown in Figure 17, the observations were also verified by slicing the specimens as shown in Figures 6 and 7. The observations from micrographs of the edges are discussed later. For specimen 10B-03, shown in Figure 18, the gray intensity is less pronounced which made it more difficult to determine how far the contrast fluid had penetrated into the damaged section. For specimen 7B-06, the delamination lengths measured at the polished edges of corners 1 to 4 were added to Figure 19. The measured lengths are listed in Table III.

Micrographs of the interior obtained from individual slices of the specimens

Two specimens (8B-06 and 10B-03) were cut into slices as discussed earlier. The slices are shown in Figures 6 and 7. The edges marked with a red star in Figure 6 were polished and micrographs were obtained to reveal the growth in the interior of the specimen. The micrographs taken across the width of specimen 8B-06 along the flange edge from corners 3 to 4 were assembled as shown in Figure 20. A detail of an x-ray radiograph (taken from Figure 16c) and a sketch of the slices (taken from Figure 6a) were included to help identify the location of the micrographs with respect to the specimen width. At the specimen edges (corners 3, z_{1l}=0.0 mm and 4, z_{4r}=25.578 mm), only one delamination type (B, in red or A1, in light blue) was observed as discussed earlier and shown in Figures 14 and 15. Based on the observations at the edges of the specimen, a simple transition from delamination type B to type A1 was expected to occur in the interior of the specimen. The micrographs, however, reveal a more complex pattern where both delaminations (B and A1) are present simultaneously across most of the width of the specimen. The mechanics of the failure are discussed below. The delamination lengths were measured using image analysis of the scanned and stiched micrographs. The delamination lengths are listed in Table IV. The delamination outline seen in the X-ray image (dark area) captured the size of the delamination well, which is shown by adding delamination lengths (B, in red or A1, in light blue) measured from the micrographs. The images obtained from X-ray radiography, however, were not able to reveal the complexity of the damage pattern observed. An ultrasound inspection, which includes a D-scan, time-of-flight scan or depth scan may be required to identify the complete pattern.

The micrographs taken across the width of specimen 8B-06 along the opposite flange edge from corners 1 to 2 were assembled in a similar manner as shown in Figure 21. As above, a detail of an x-ray radiograph and a sketch of the slices were included to help identify the location of the micrographs with respect to the specimen width. The same complex pattern as discussed above is observed where both delaminations (B, in yellow and A1, in magenta) are present simultaneously across most of the width of the specimen. In this particular case, delamination A1 is visible across the entire width of the specimen including the free surface at corner 2 (z_{4r}=25.578 mm). The delamination lengths measured from the individual micrographs are listed in Table IV. The lengths listed in Table III and Table IV for the same corners differ slightly, since they were measured at

different times using different equipment.

The micrographs taken across the width of specimen 10B-03 along the flange edge from corners 3 to 4 were assembled as discussed above and are shown in Figures 22a and b. A detail of an x-ray radiograph (taken from Figure 17d) and a sketch of the slices (taken from Figure 6b) were included to help identify the location of the micrographs with respect to the specimen width. The same complex pattern as discussed above for specimen 8B-06 is observed here, and both delaminations (B, in yellow and A1, in magenta) are present simultaneously across most of the width of the specimen. The delamination lengths measured at the edges are listed in Table III.

The assembly of the corresponding micrographs taken across the width of the specimen along the opposite flange edge from corners 1 to 2 is shown in Figures 23a and b. The same complex pattern as discussed above is observed here, and both delaminations (B, in yellow and A1, in magenta) are present simultaneously across most of the width of the specimen.

Mechanics of Failure

Earlier investigations [2-5] indicated that the maximum ply principal transverse tensile stress may cause the initial failure in the form of matrix cracks from which delaminations may start to grow. Failure, therefore, may occur when the computed principal tensile stress in the plane normal to the fiber direction exceeds the transverse tensile strength of this ply. Due to geometric symmetry of the specimen and the tensile loading, one would therefore expect to see the same type of matrix cracking simultaneously at all four corners of the flange. Due to the presence of +45° and -45° plies in the layup, however, the specimen is not symmetric resulting in a failure pattern that is not symmetric. The observed matrix cracking and delamination growth is the same at diagonally opposite corners of the flange e.g. 1 and 4 or 2 and 3 as shown in Figures 14 and 15.

Previous two and three-dimensional finite element analyses of the current specimen configuration accounted for different locations where the first delamination might occur, however, were based on the assumption that delamination occurred only in one interface across the entire width of the specimen [7-9]. A more comprehensive understanding of the complex mechanics of the failure process would require modeling delaminations simultaneously at different interfaces to determine the propagation and growth of the individual delamination. Such detailed three-dimensional finite element analyses, however, are out of the scope of this paper.

SUMMARY AND CONCLUDING REMARKS

The fatigue damage was characterized in specimens which consisted of a tapered composite flange, representing a stringer or frame, bonded onto a composite skin. In the first step, a quasi-static tension test was performed to determine the failure load. Subsequently, tension fatigue tests were performed at 40%, 50%, 60% and 70% of the failure load to evaluate the debonding mechanisms between the skin and the bonded stringer. For four specimens, the cycling loading was stopped at intervals, and the specimens were taken out of the grips. Photographs of the polished specimen edges were taken under a light microscope to document the occurrence and growth of matrix cracks and delaminations. Additionally, dye penetrant X-ray radiography was used to measure

the amount of delamination through the width. In addition, two specimens were cut longitudinally into several sections. Photographs of the polished section edges were taken under a light microscope to document the damage inside the specimens.

The microscopic inspection revealed the following:

- All quasi-static and fatigue tests yielded similar damage patterns. Under quasi-static loading, failure occurred across one flange tip of the specimen only, with no clear preference for corners 1 and 2 or corners 3 and 4. In fatigue, damage initiated at both flange tips, but not at the same time.
- At corners 2 and 3, a delamination initiated at the flange tip from a matrix crack in the top 45° skin ply and propagated in the top 45°/-45° skin ply interface. In fatigue, damage first appeared at this location for 12 of the 14 specimens.
- At corners 1 and 4, a delamination running in the bondline initiated from a matrix crack in the adhesive pocket.
- The micrographs taken from individual slices reveal a more complex pattern inside the specimen. The two delamination patterns observed at the edges are present simultaneously across most of the width of the specimen.
- The outline from the X-ray images compared well with lengths measured from the micrographs taken from individual slices. Images obtained from X-ray radiography, however, did not reveal the complexity of the damage pattern.

The observations suggest that a more sophisticated nondestructive evaluation technique such a D-scan, time-of-flight scan or depth scan is required to capture the complex damage pattern of matrix cracking and multi-level delaminations. With respect to finite element modeling of delaminations and predicting their propagation and growth, the question arises of how much simplification is permissible and how much detail is required in order to properly capture the damage mechanism.

REFERENCES

[1] P.J. Minguet, M.J. Fedro, T.K. O'Brien, R.H. Martin, and L.B. Ilcewicz, *Development of a Structural Test Simulating Pressure Pillowing Effects in a Bonded Skin/Stringer/Frame Configuration*, in Proceedings of the Fourth NASA/DoD Advanced Composite Technology Conference, Salt Lake City, Utah, 1993.

[2] P.J. Minguet and T.K. O'Brien, *Analysis of Composite Skin/Stringer Bond Failures Using a Strain Energy Release Rate Approach*, in The Tenth International Conference on Composite Materials, vol. I, A. Poursartip and K. Street, Eds., pp. 245-252, 1995

[3] P.J. Minguet and T.K. O'Brien, *Analysis of Test Methods for Characterizing Skin/Stringer Debonding Failures in Reinforced Composite Panels*, in Composite Materials: Testing and Design (Twelfth Volume), ASTM STP 1274, pp. 105-124, 1996.

[4] P.J. Minguet, *Analysis of the Strength of the Interface Between Frame and Skin in a Bonded Composite Fuselage Panel*, in The 38rd AIAA/ASME/ASCE/AHS/ASC Structures, Structural Dynamics and Materials Conference, pp. 2783-2790, 1997.

[5] R. Krueger, M.K. Cvitkovich, T.K. O'Brien, and P.J. Minguet, *Testing and Analysis of Composite Skin/Stringer Debonding Under Multi-Axial Loading*, Journal of Composite Materials, vol. 34, pp. 1263-1300, 2000.

[6] M.K. Cvitkovich, T.K. O'Brien, and P.J. Minguet, *Fatigue Debonding Characterization in Composite Skin/Stringer Configurations*, in Composite Materials: Fatigue and Fracture, Seventh Volume, ASTM STP 1330: American Society for Testing and Materials, pp. 97-121, 1998.

[7] R. Krueger, I.L. Paris, T.K. O'Brien, and P.J. Minguet, *Fatigue Life Methodology for Bonded Composite Skin/Stringer Configurations*, Journal of Composites Technology and Research, vol. 24, pp. 56-79, 2002.

[8] I.L. Paris, R. Krueger, and T.K. O'Brien, *Effect of Assumed Damage and Location on the Delamination Onset Predictions for Skin-Stiffener Debonding*, AHS Journal, vol. 49, pp. 501-507, 2004.

[9] R. Krueger, I.L. Paris, T.K. O'Brien, and P.J. Minguet, *Comparison of 2D Finite Element Modeling Assumptions with Results from 3D Analysis for Composite Skin-Stiffener Debonding*, Composite Structures, vol. 57, pp. 161-168, 2002.

TABLE I. OVERVIEW OF TEST SPECIMENS.

Specimen	Load level[¶]	Panel number[*]	Slice No. i	Slice width w_i, mm	Distance from edge z_{il}, mm	Distance from edge z_{ir}, mm
9B-02[+]	70%	2				
6B-02	70%	2				
4B-03	70%	3				
6B-03	70%	3				
8B-06[+]	70%	6	1	6.637	0.000[++]	6.637[++]
			2	6.310	7.220	13.530[++]
			3	6.037	14.110[++]	20.147[++]
			4	4.855	20.723	25.578[++]
7B-02	60%	2				
11B-02	60%	2				
7B-03	60%	3				
9B-03	60%	3				
3B-06	60%	6				
7B-06[+]	60%	6				
8B-02	50%	2				
12B-02	50%	2				
5B-03	50%	3				
10B-03[+]	50%	3	1	3.560	0.000[++]	3.560[++]
			2	3.328	3.912	7.240[++]
			3	3.023	7.565	10.588[++]
			4	3.461	10.949	14.410[++]
			5	3.342	14.810	18.152[++]
			6	3.423	18.499	21.922[++]
			7	3.060	22.303	25.363[++]
4B-06	50%	6				
10B-02	40%	2				
8B-03	40%	3				
11B-03	40%	3				
12B-03	40%	3				
11B-06	40%	6				

[*] Panel 2: [45/-45/0/-45/45/90/90/0/45/0/45/-45]; 3 and 6: [45/-45/0/-45/45/90/90/-45/45/0/45/-45]

[¶] Load level 70%=12.45 kN, 60%=10.67 kN, 50%=8.9 kN, 40%=7.12 kN

[+] X-rays taken for four specimens

[++] Polished edges

TABLE II. RESULTS FOR QUASI-STATIC TENSION TESTS.

Specimen	Damage initiation load, kN	Damage initiation flange strain, με	Damage initiation skin strain, με	Max. load, kN	Flange strain at max. load, με	Skin strain at max. load, με
2B02	19.9	1368	9934	19.9	1368	9934
2B03	15.9	1075	9756	17.2	577	10280
2B06	16.6	1153		17.7	704	
6B06	18.3	1390		18.3	1390	
10B06	18.0	1378		18.0	1378	
mean	17.8	1273	9845	18.2	1083	10107
std. dev.	1.6	148	126	1.0	407	245
CoV [%]	8.9	11.6	1.3	5.7	37.6	2.4

TABLE III. DELAMINATION LENGTHS AT CORNERS 1-4.

Specimen – load level	Number of cycles	Corner 1 a_{c1}, mm	Corner 2 b_{c2}, mm	Corner 3 b_{c3}, mm	Corner 4 a_{c4}, mm
9B-02 – 70%	1400	MC	3.99	1.297	MC
	1995	2.415	5.877	5.05	0.386
	5000	3.869	9.536	8.475	2.418
7B-06 – 60%	3233	MC	MC	3.972	-
	4460	0.804	3.264	5.779	2.557
8B-06 – 70%	279	0.301	MC	2.156	MC
	506	0.307	MC	5.027	MC
	730	0.681	2.34	7.87	1.1
10B-03 – 50%	5502	MC(0.512)	1.827	MC	MC (0.786)
	6506	MC	3.823	MC	MC
	7611	MC	4.431	2.265	MC
	11500	1.676	7.58	5.699	2.083

MC: matrix crack only – damage has not yet developed into a delamination

TABLE IV. DELAMINATION LENGTHS FOR SLICED SPECIMENS.

Specimen	Load level	Slice No. *i*	**Edge from corner 3 to 4**		**Edge from corner 1 to 2**	
			length A1, mm	length B, mm	length A1, mm	length B, mm
8B-06	70%	1	a_{1l}=0.00	b_{1l}=8.20	a_{1l}=0.71	b_{1l}=0.00
			a_{1r}=1.34	b_{1r}=5.13	a_{1r}=1.03	b_{1r}=0.70
		2	a_{2r}=2.37	b_{2r}=2.95	a_{2r}=1.22	b_{2r}=1.37
		3	a_{3l}=1.55	b_{3l}=4.21	a_{3l}=0.68	b_{3l}=1.01
			a_{3r}=1.09	b_{3r}=1.80	a_{3r}=0.34	b_{3r}=2.97
		4	a_{4r}=1.05	b_{4r}=0.00	a_{4r}=0.46	b_{4r}=2.60

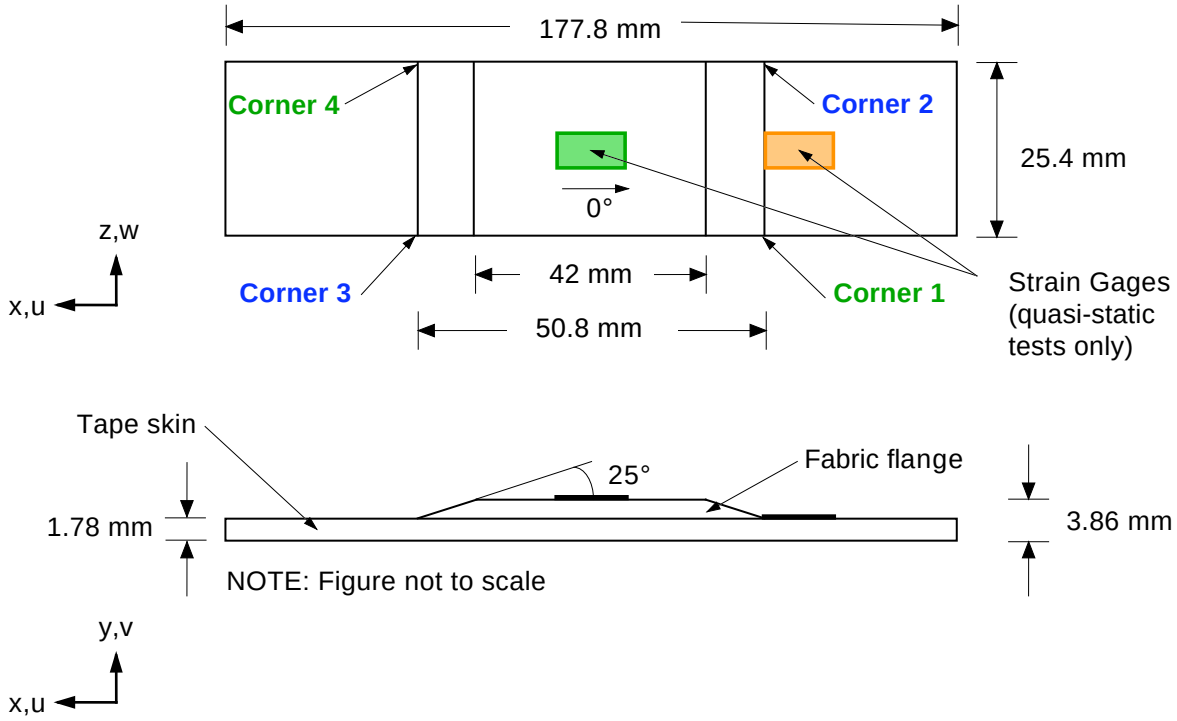

(a). *Specimen configuration.*

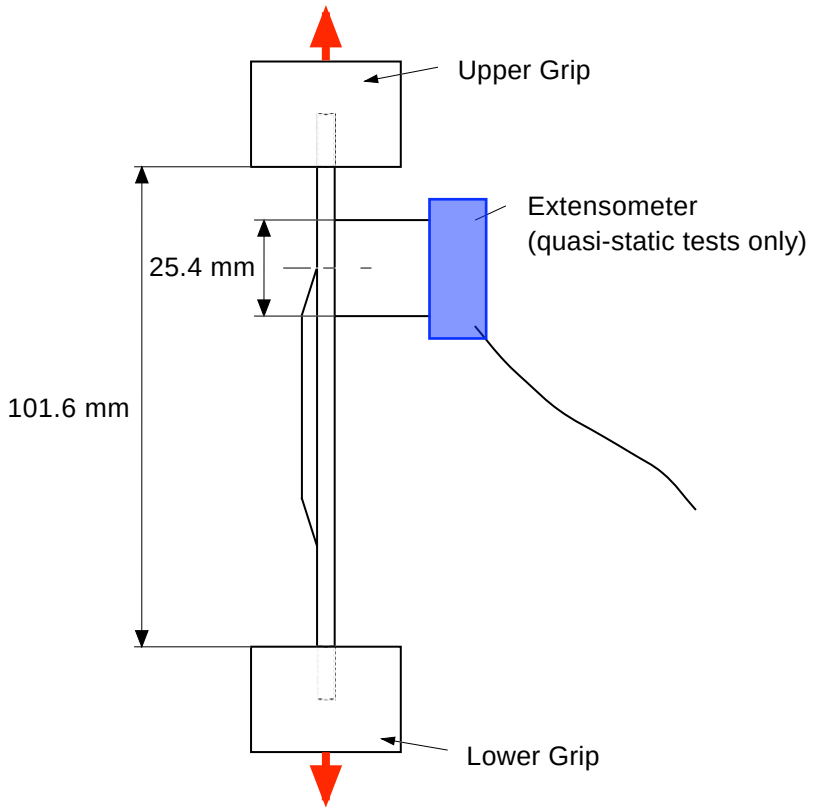

(b). *Tension test set-up.*

Figure 1. *Specimen configuration and test set-up [5,7].*

(a). *Test set-up.*

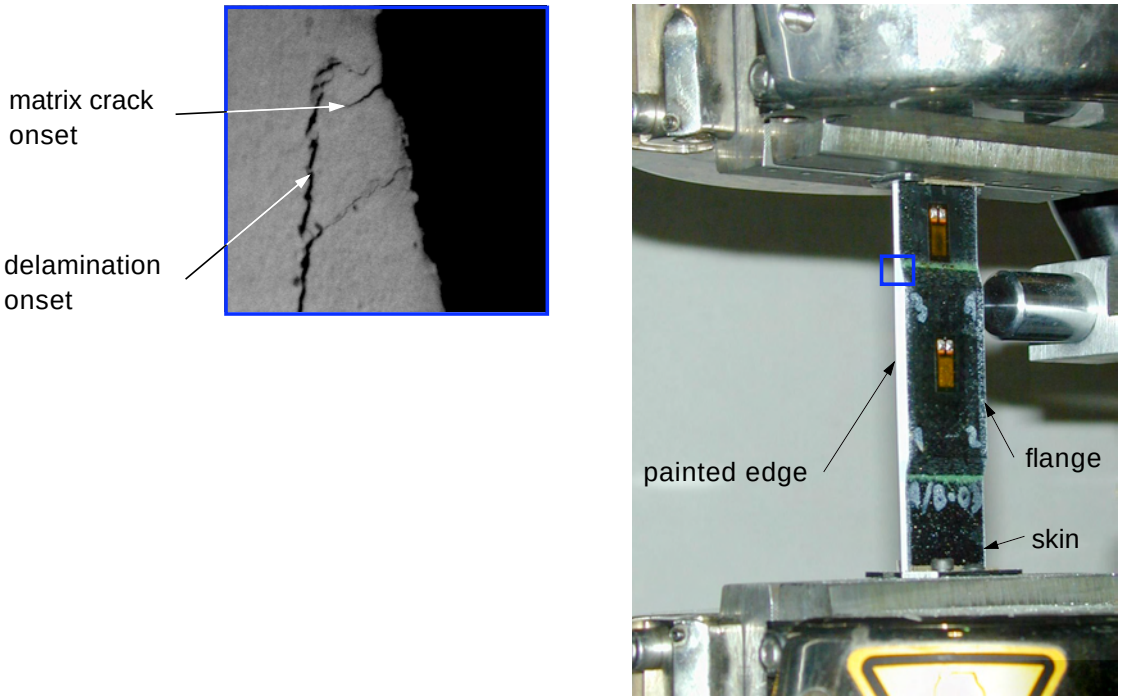

(b). *Specimen in the loading grips.*

Figure 2. *Fatigue tension test set-up.*

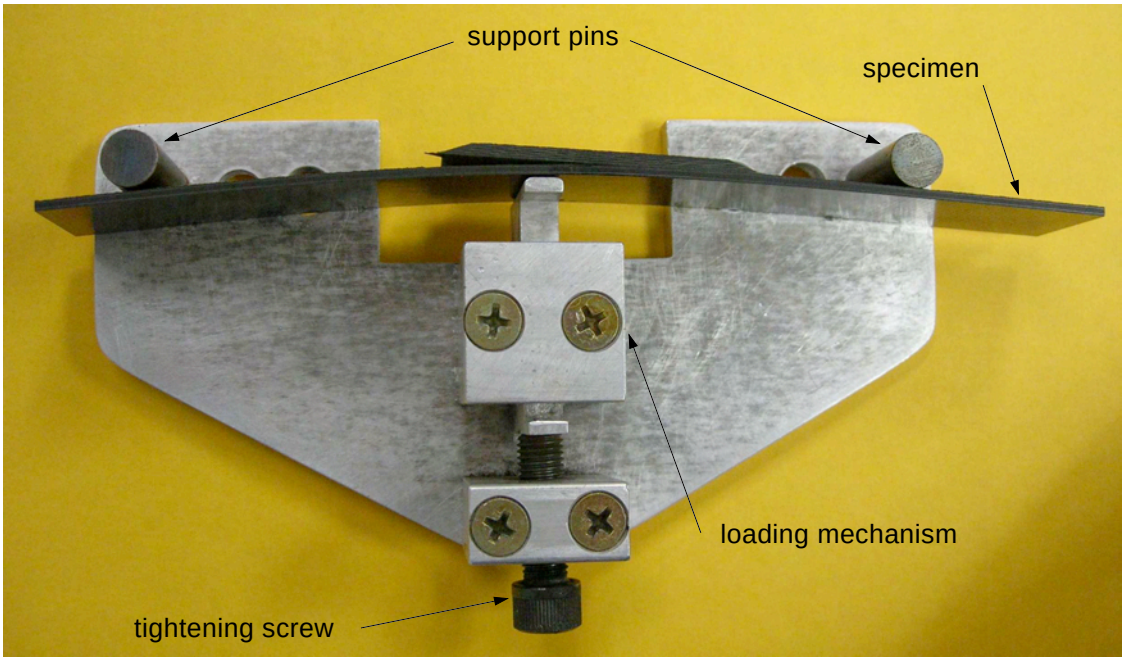

(a). *Loaded specimen in the rig.*

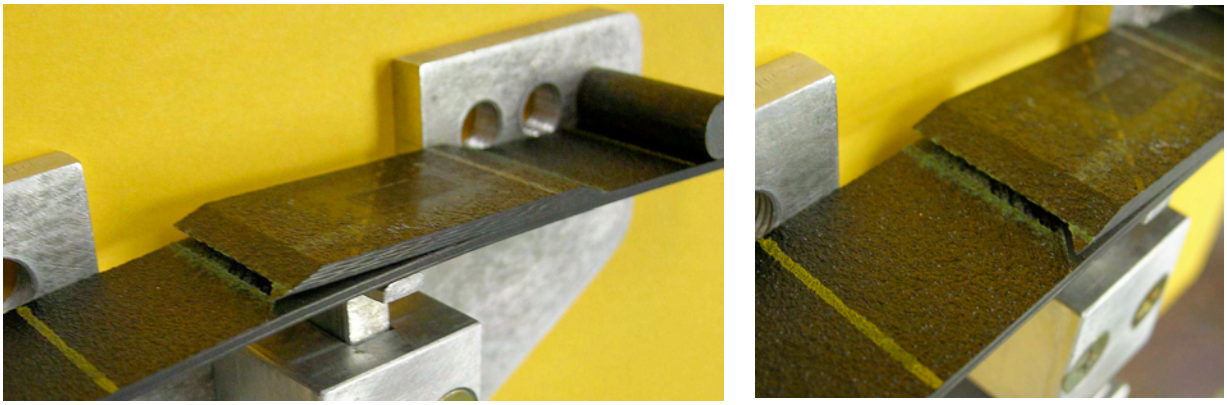

(b). *Detail of observed delamination opening.*

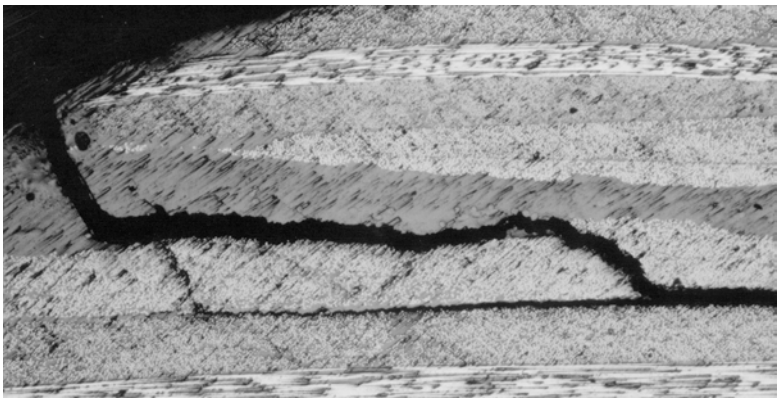

(c). *Photograph of polished edge.*

Figure 3. *Three-point bending rig.*

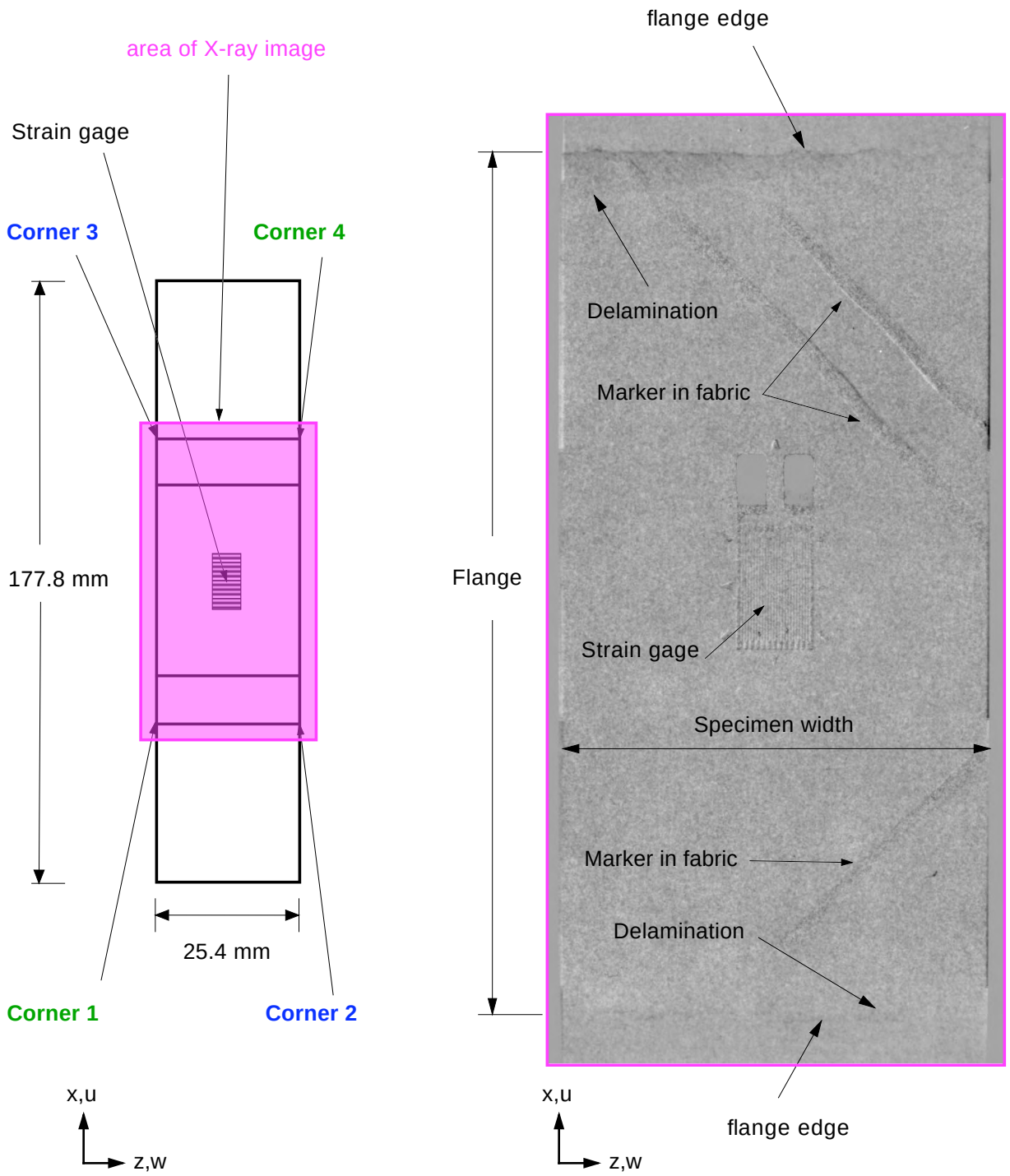

(a) *Top view of specimen*

(b) *X-ray radiograph of specimen 8B-06 taken after 279 load cycles*

Figure 4. *X-ray radiograph of skin/stringer specimen.*

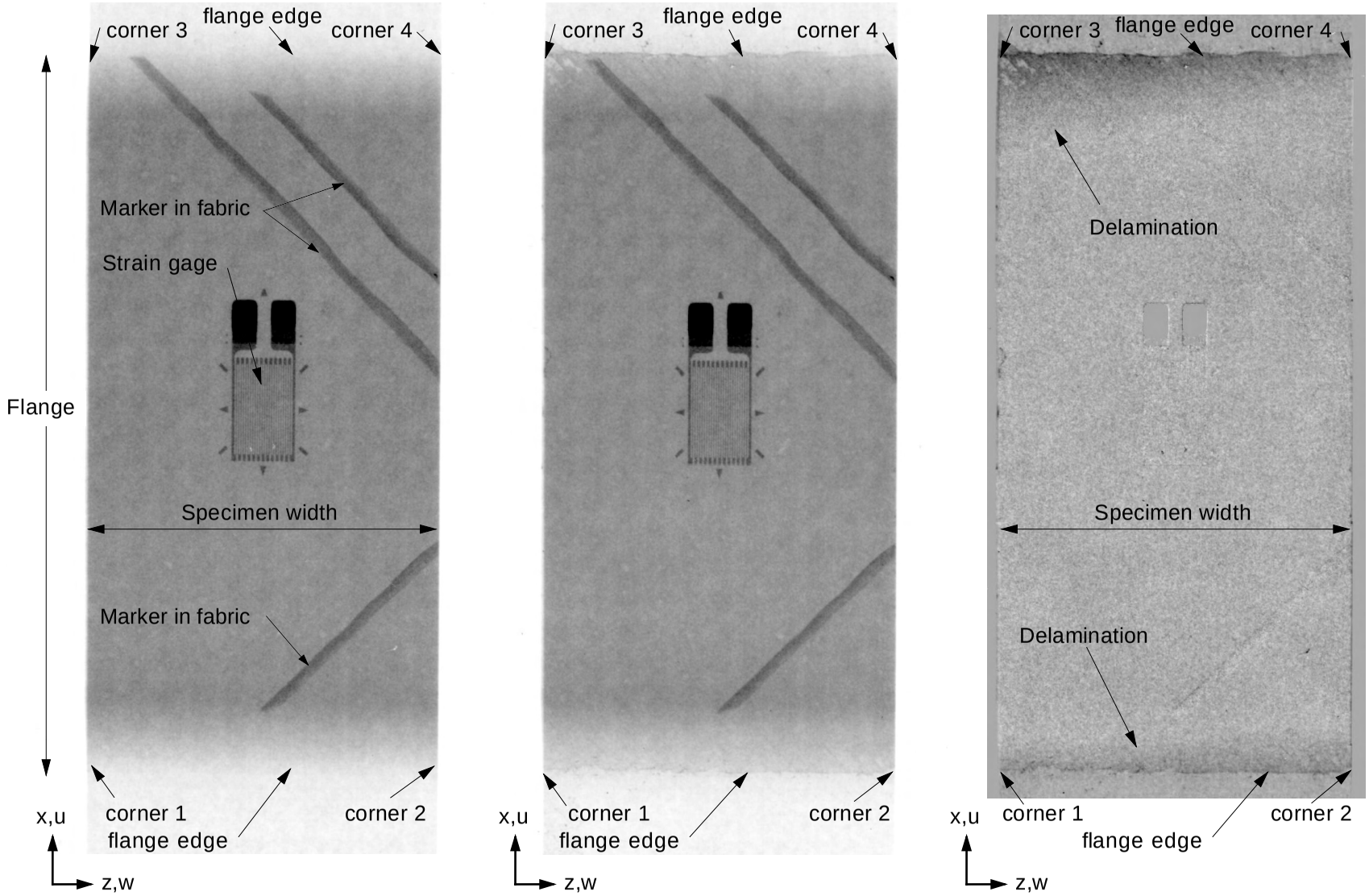

(a) *X-ray radiograph of undamaged specimen*

(b) *X-ray radiograph of damaged specimen*

(c) *Final enhanced image of damage*

Figure 5. *Image processing of X-ray radiographs (specimen 8B-06 after 730 cycles).*

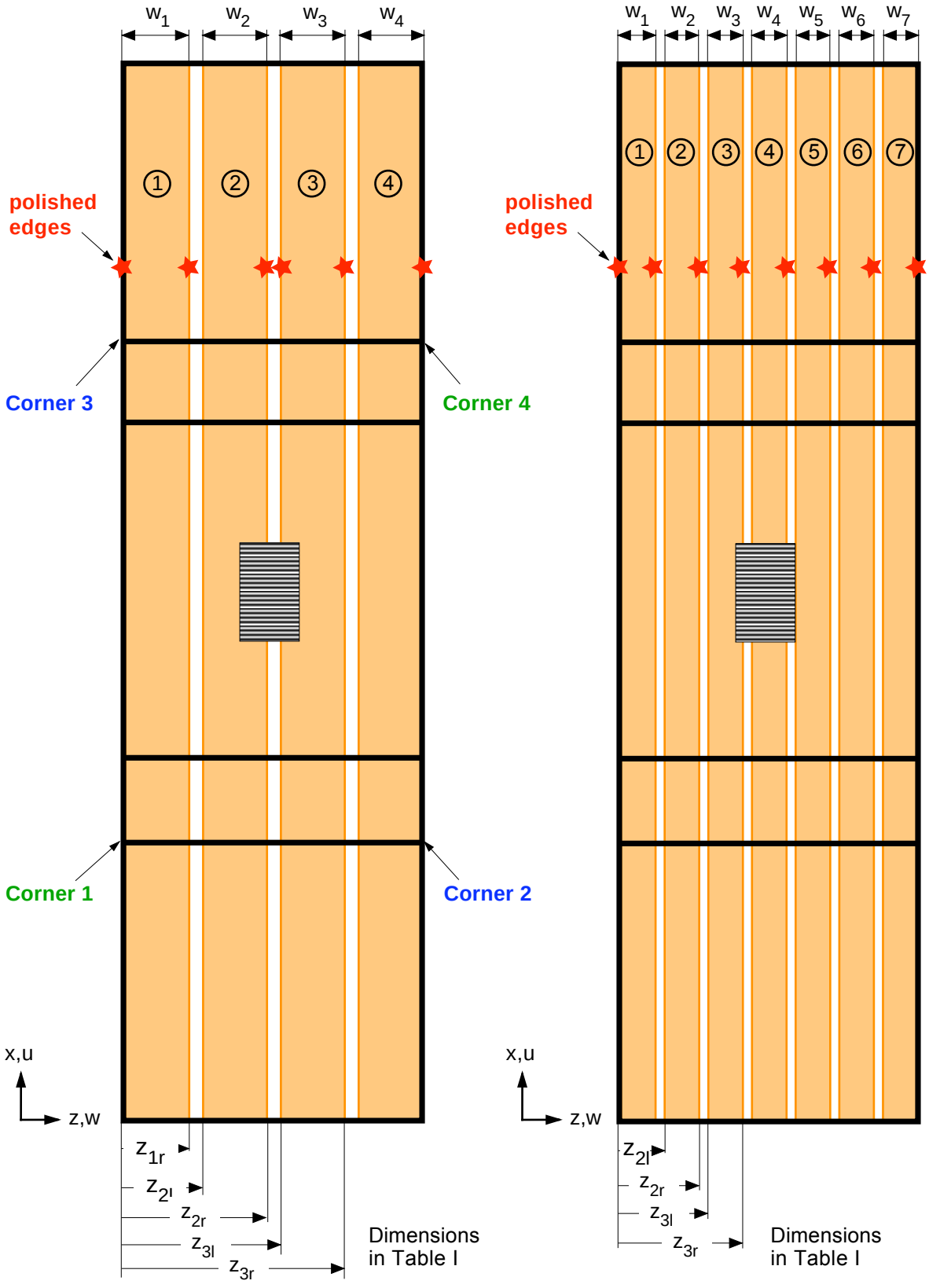

(a) *Specimen 8B-06* (b) *Specimen 10B-03*

Figure 6. *Cutting of specimens.*

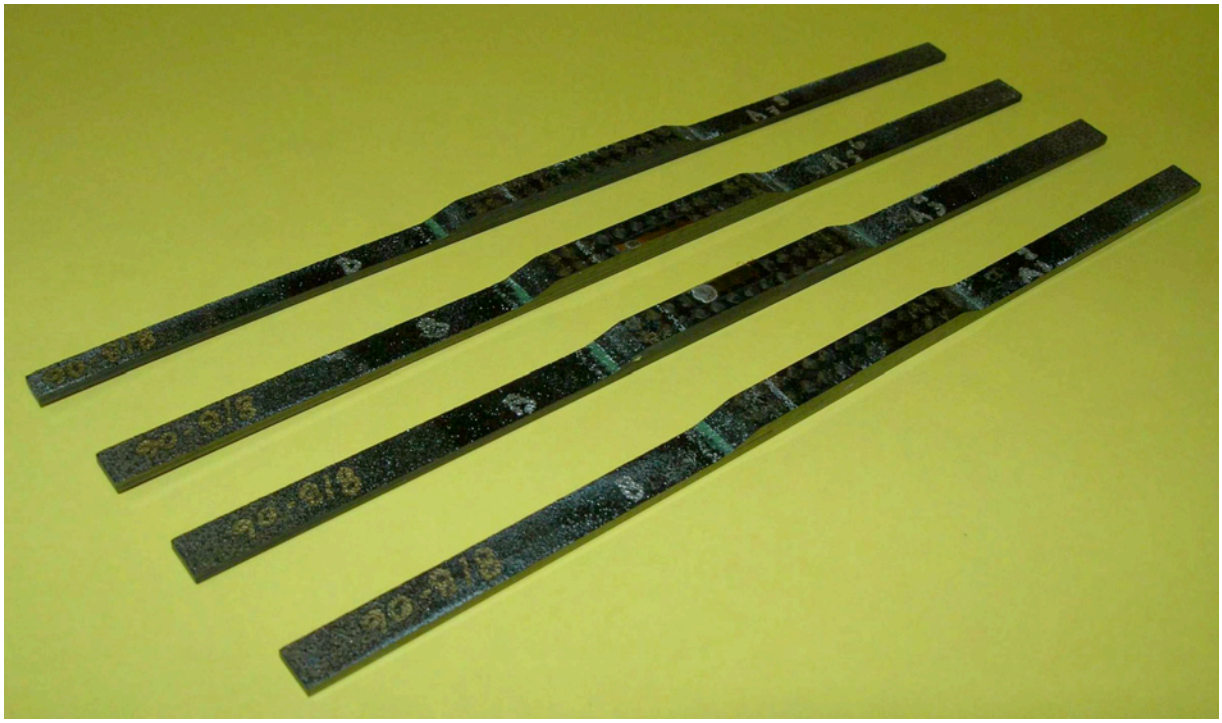

(a). *Specimen 8B-06 cut into four slices.*

(b). *Specimen 10B-03 cut into seven slices.*

Figure 7. *Sectioned specimens.*

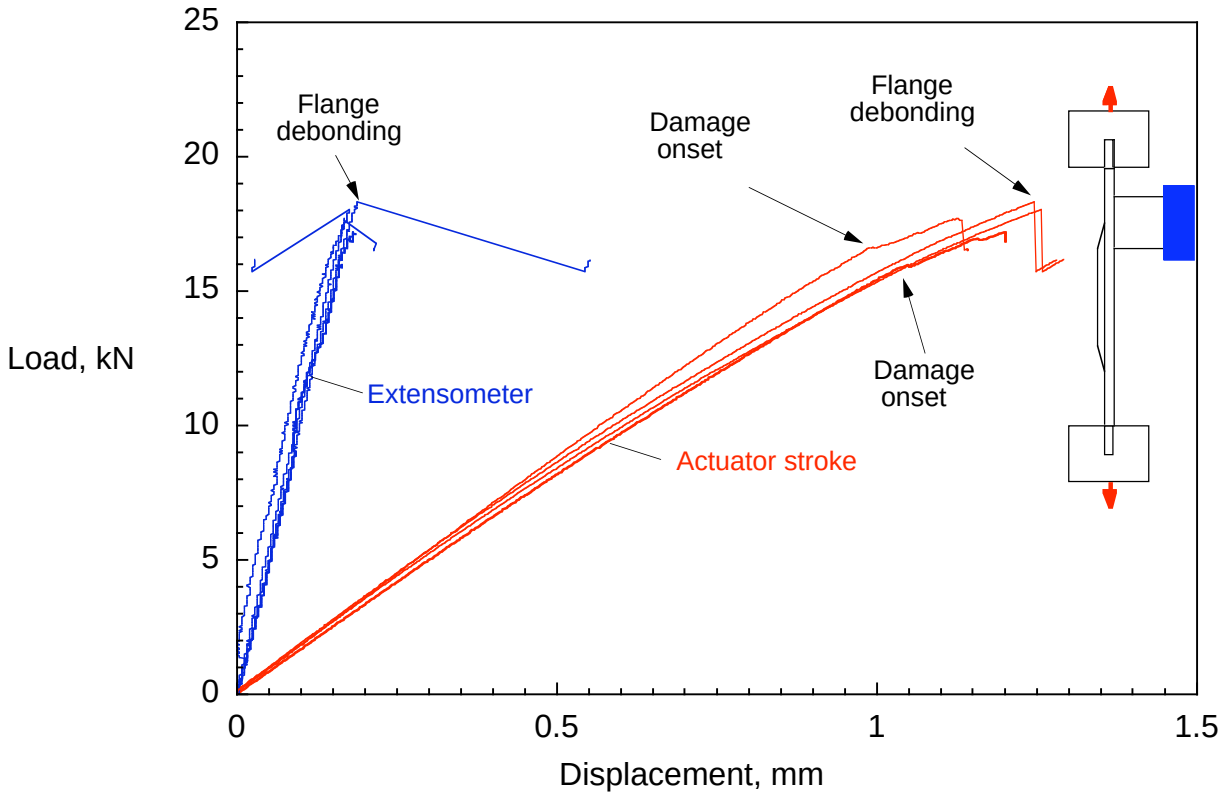

Figure 8. *Load-displacement plots for quasi-static tenstion tests [7].*

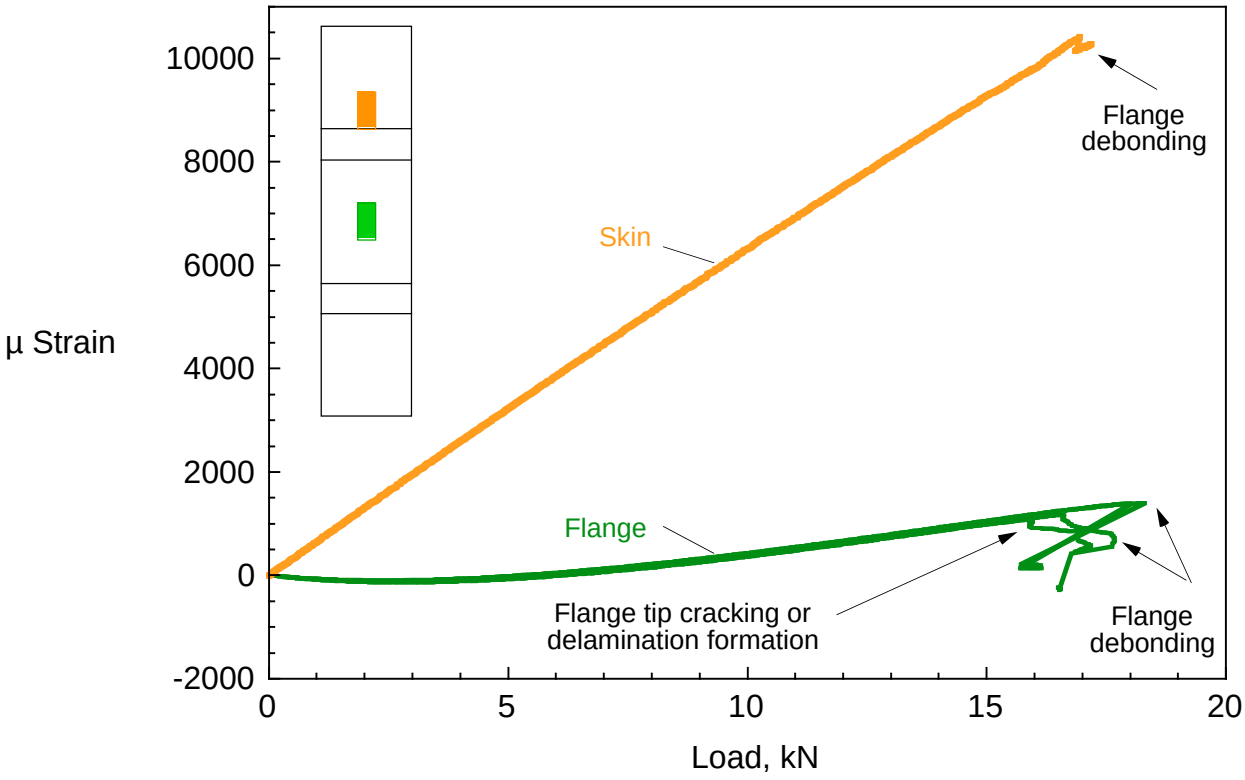

Figure 9. *Flange strain-load plots for quasi-static tension tests [7].*

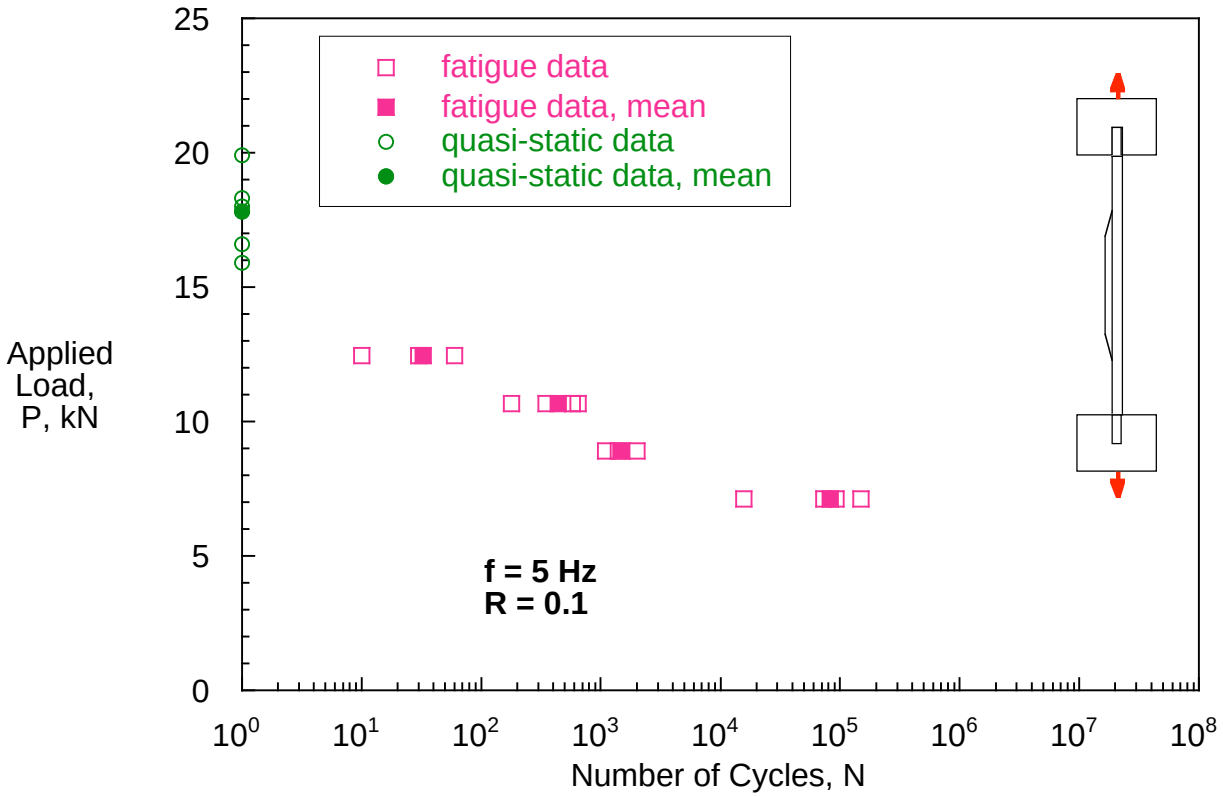

Figure 10. *Matrix crack onset fatigue life for composite skin/flange debonding [7].*

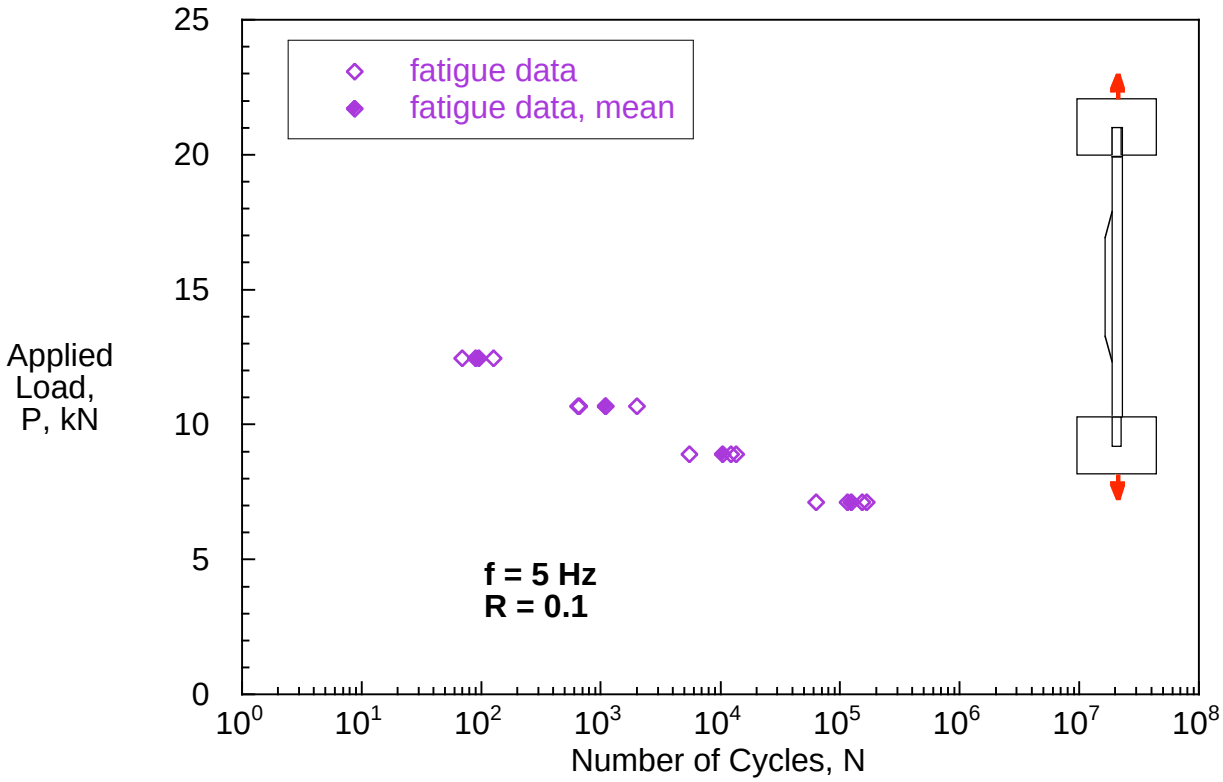

Figure 11. *Delamination onset fatigue life following matrix cracking for composite skin/flange debonding [7].*

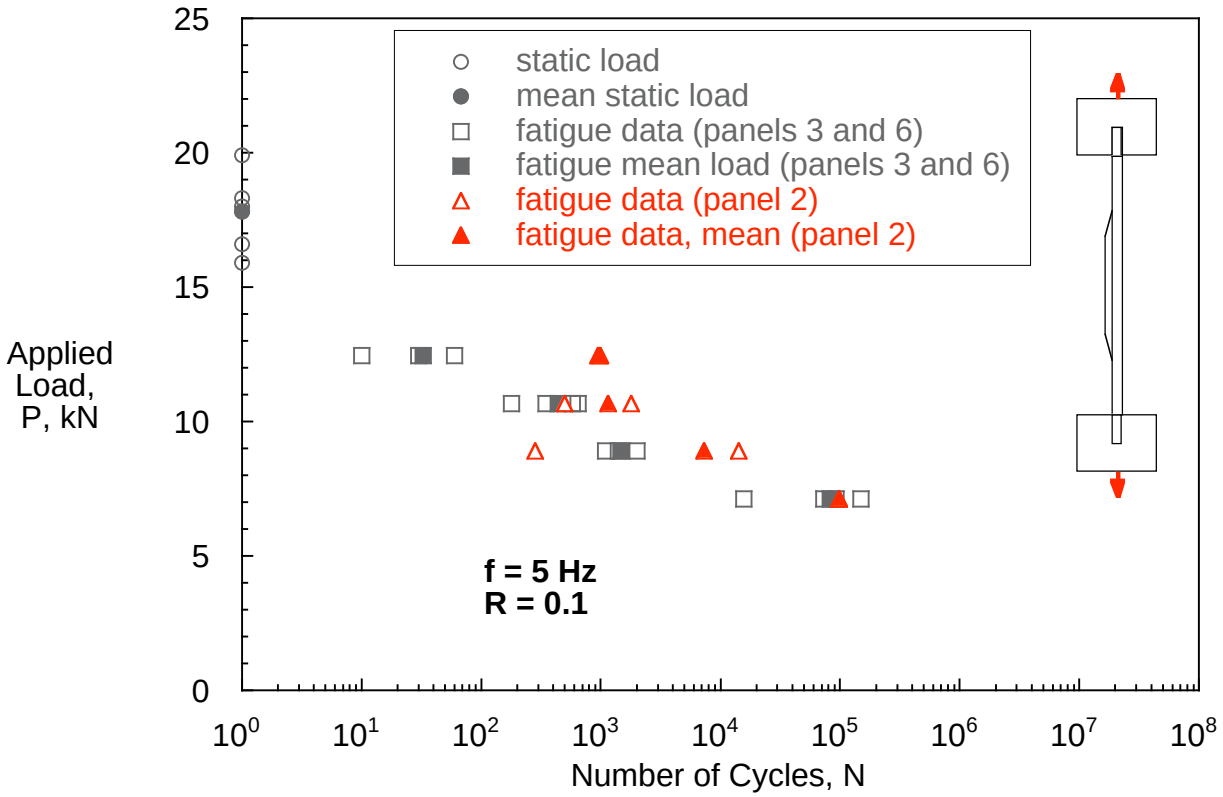

Figure 12. *Matrix crack onset fatigue life for composite skin/flange debonding for panel 2.*

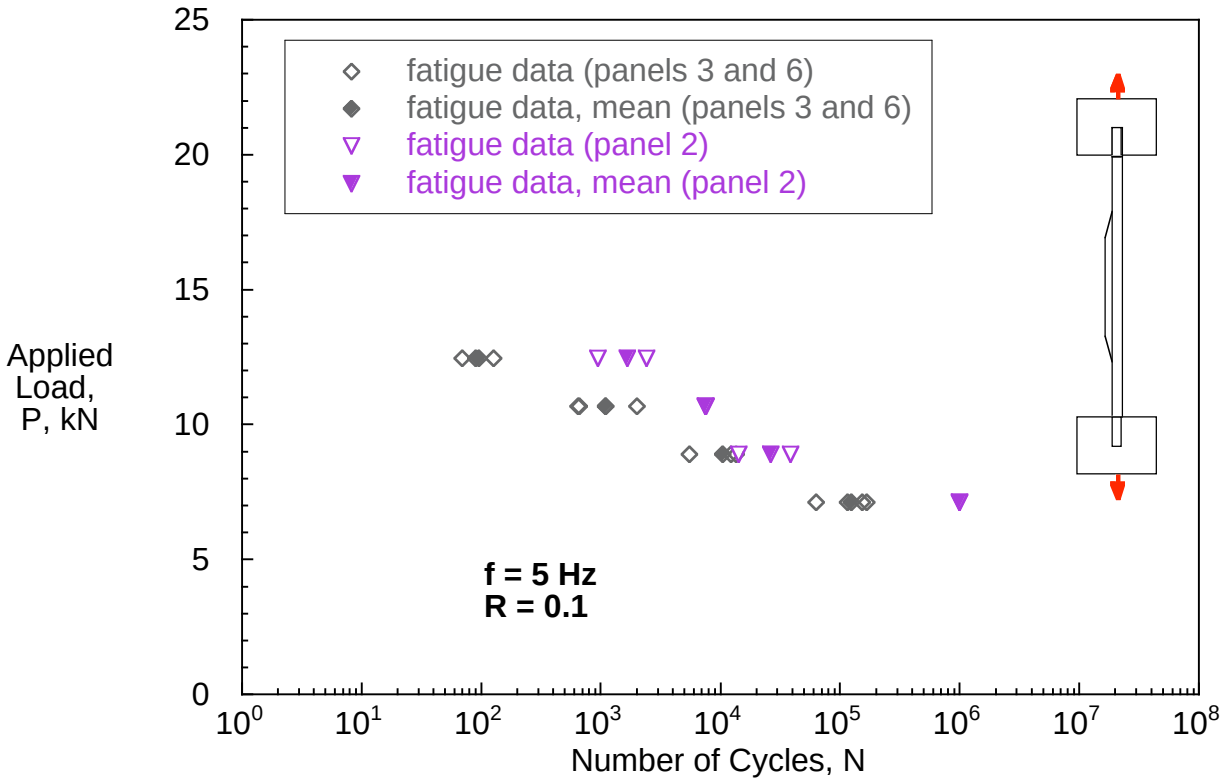

Figure 13. *Delamination onset fatigue life following matrix cracking for composite skin/flange debonding for panel 2.*

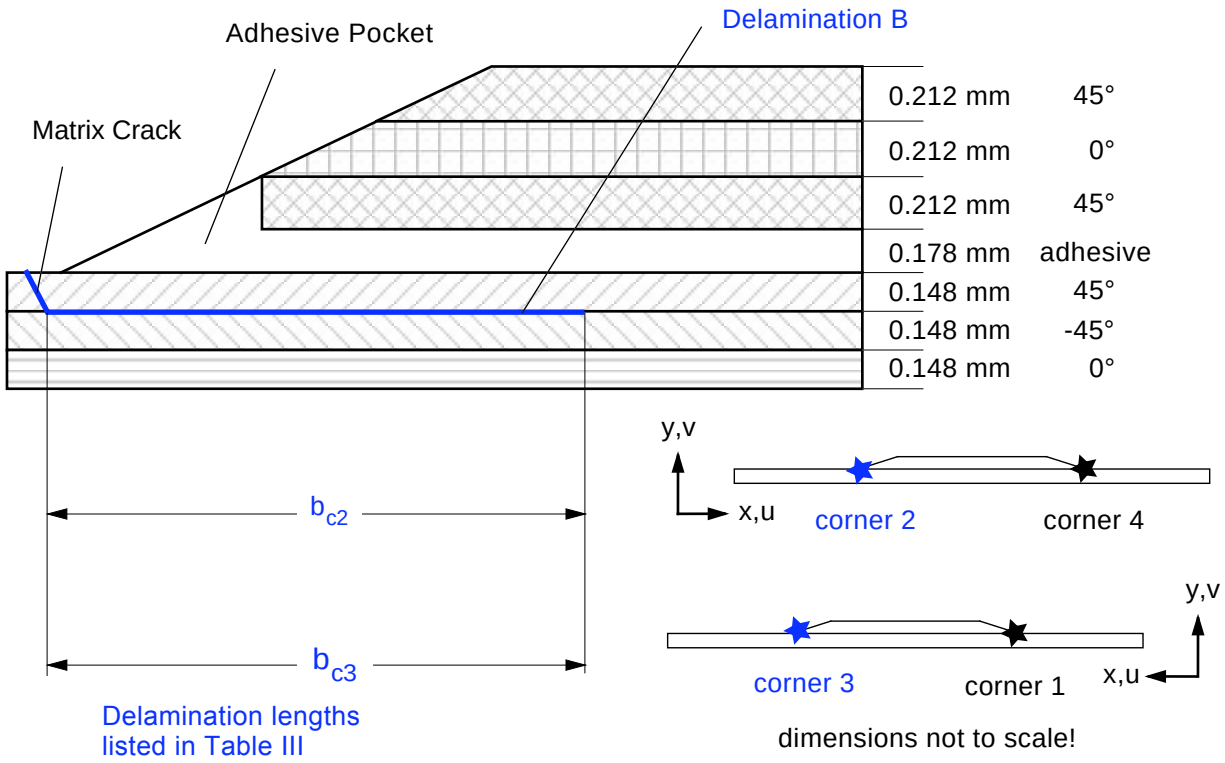

(a). *Typical damage patterns.*

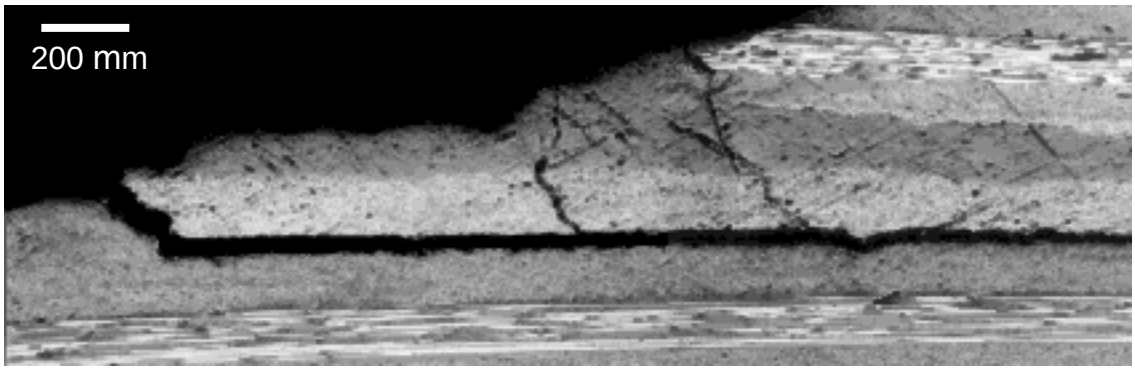

(b). *Micrograph of the edge of the failed specimen.*

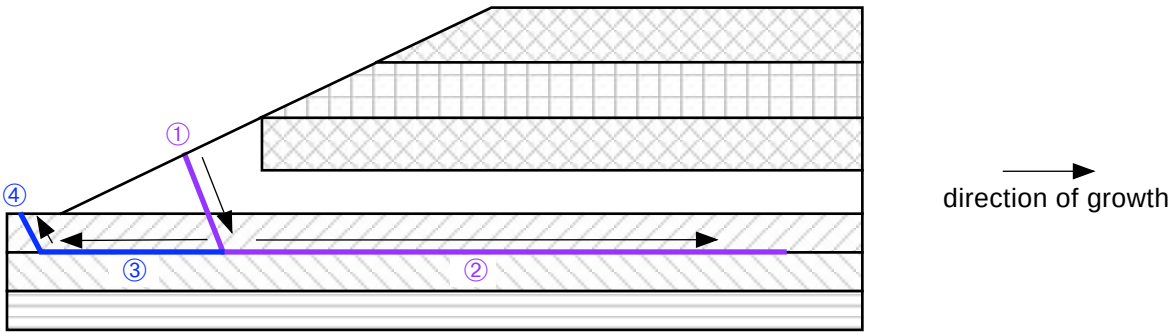

(c). *Sequence of events observed during fatigue testing.*

Figure 14. *Typical damage patterns observed in skin/stringer specimen at specimen corners 2 and 3 [7].*

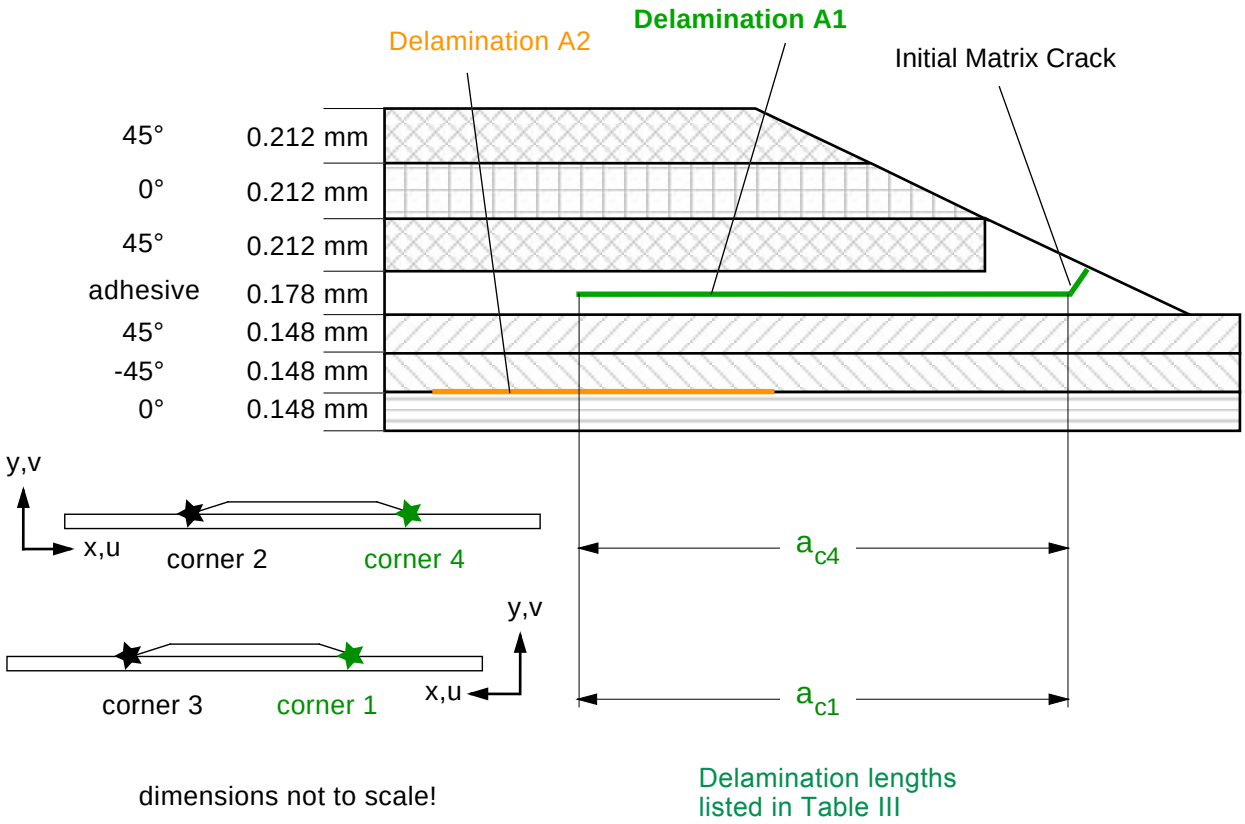

(a). *Typical damage patterns.*

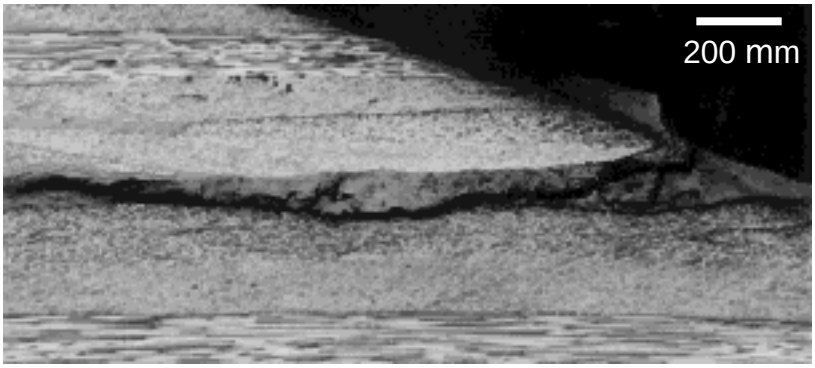

(b). *Micrograph of the edge of the failed specimen.*

Figure 15. *Typical damage patterns observed in skin/stringer specimen at specimen corners 1 and 4 [7].*

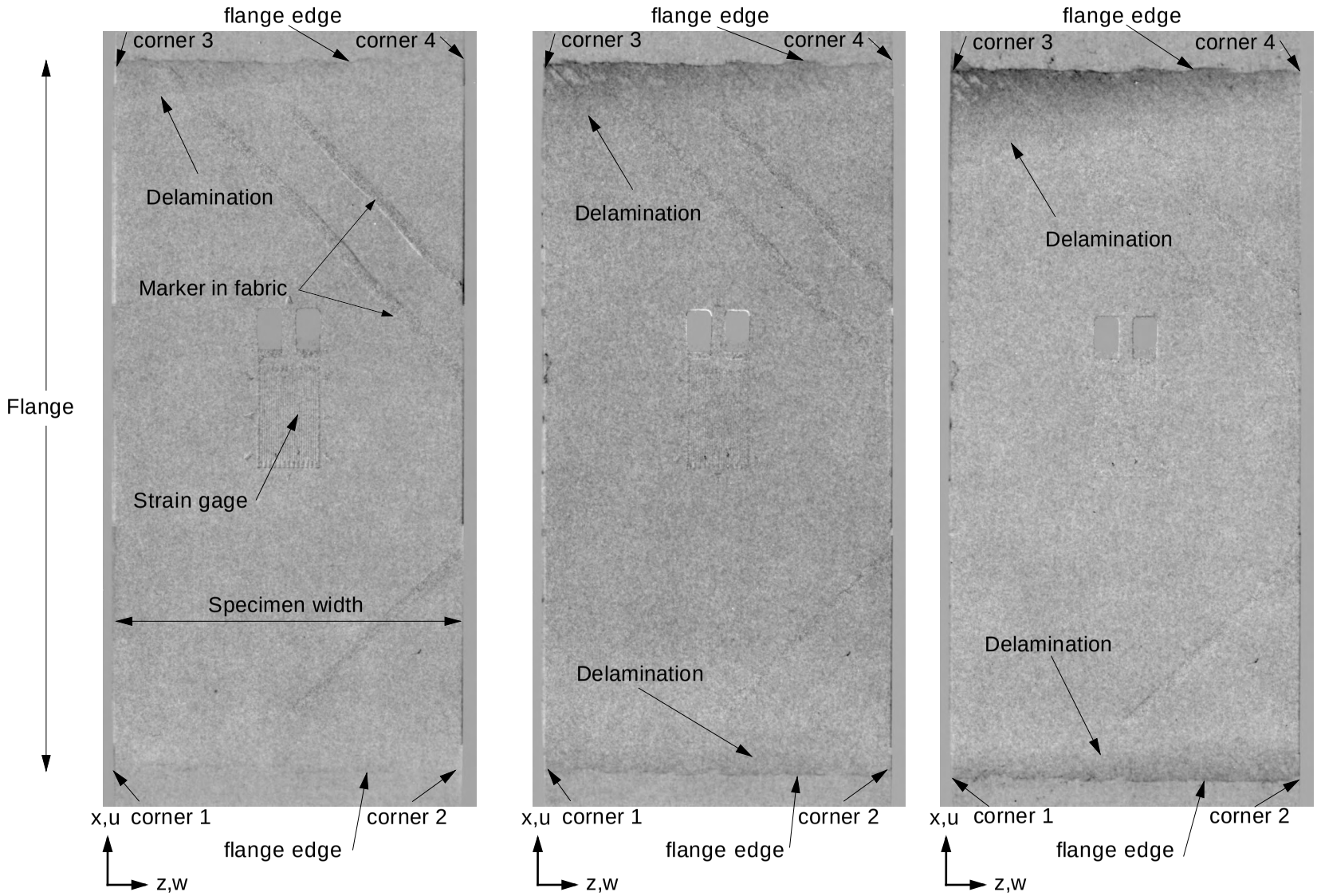

(a) *X-ray photography of flange section taken after 279 cycles*

(b) *X-ray photography of flange section taken after 506 cycles*

(c) *X-ray photography of flange section taken after 730 cycles*

Figure 16. *Damage progression in skin/stringer debond specimen 8B-06.*

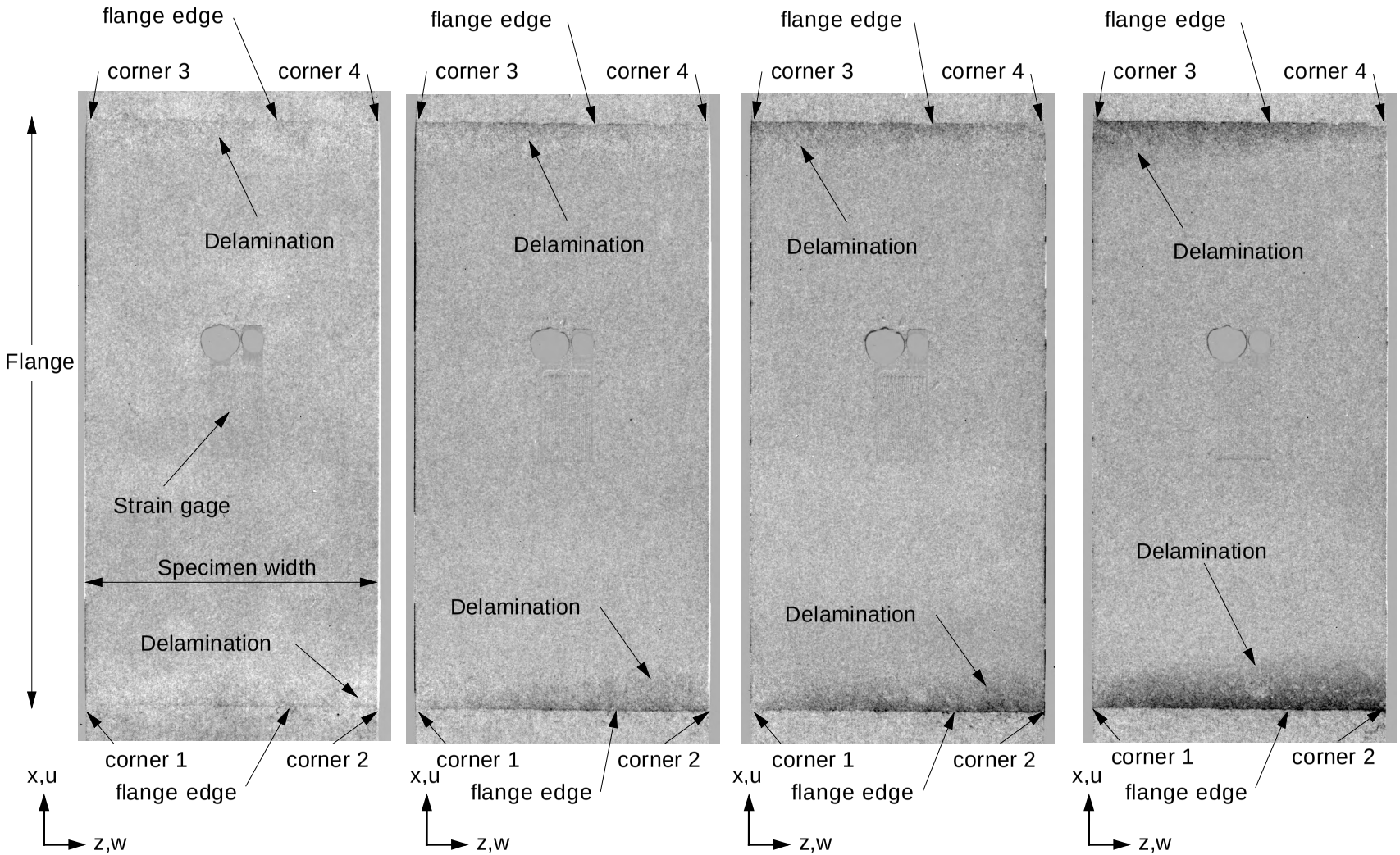

(a) *X-ray photography of flange section taken after 5502 cycles* (b) *X-ray photography of flange section taken after 6506 cycles* (c) *X-ray photography of flange section taken after 7611 cycles* (d) *X-ray photography of flange section taken after 11500 cycles*

Figure 17. *Damage progression in skin/stringer debond specimen 10B-03.*

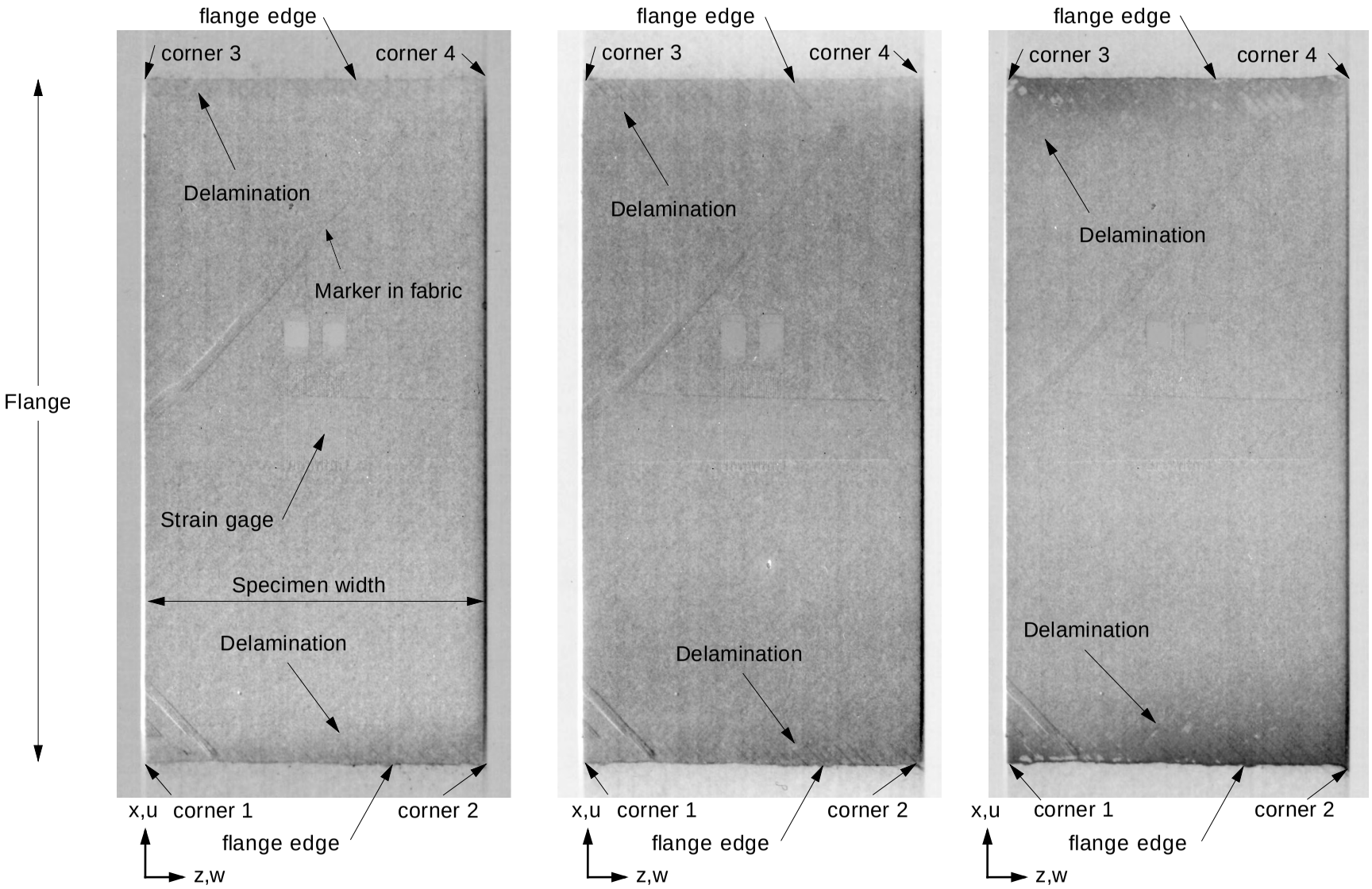

(a) *X-ray photography of flange section taken after 1400 cycles*

(b) *X-ray photography of flange section taken after 1995 cycles*

(c) *X-ray photography of flange section taken after 5000 cycles*

Figure 18. *Damage progression in skin/stringer debond specimen 9B-02.*

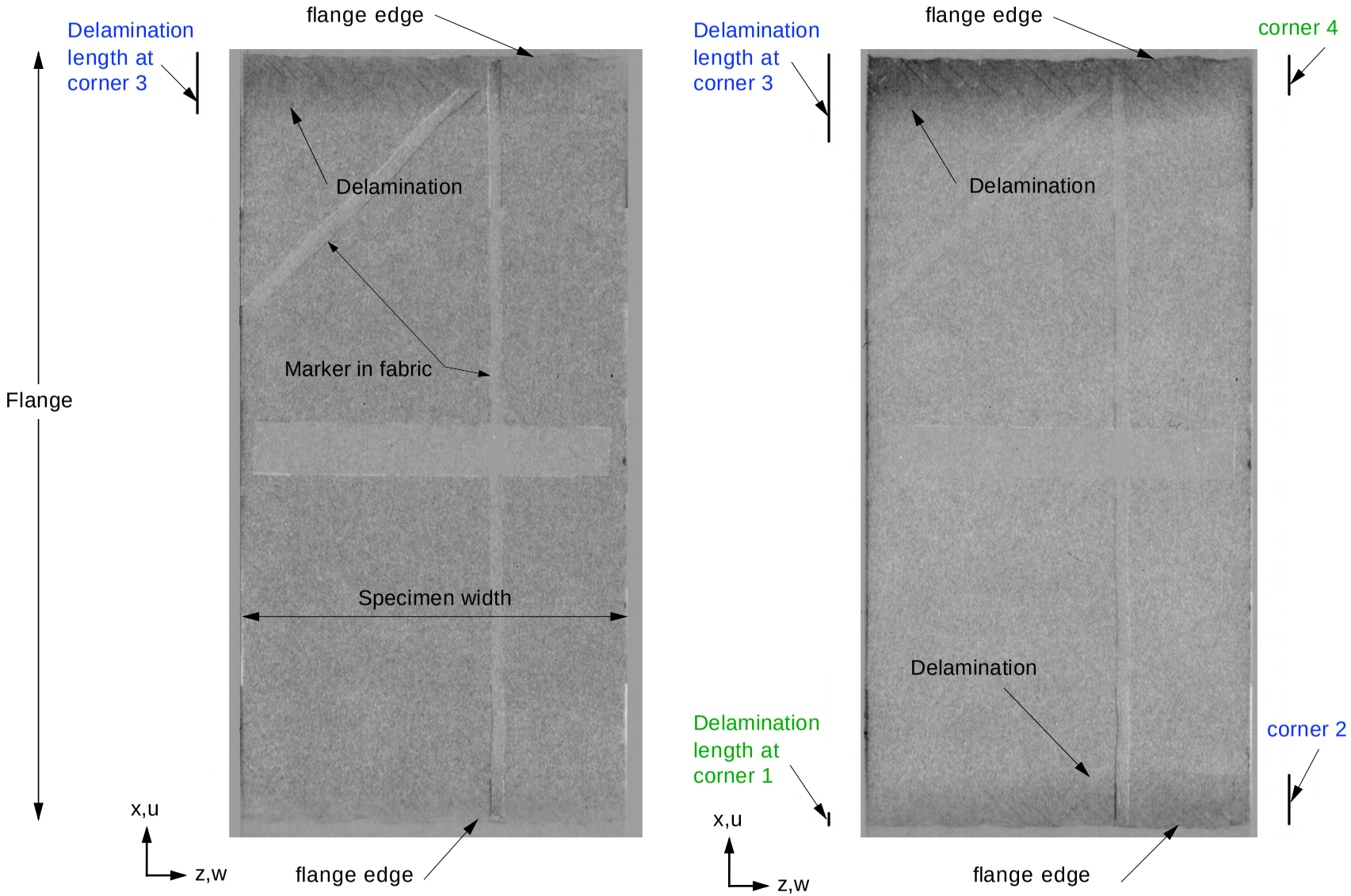

(a) *X-ray photography of flange section taken after 3233 cycles* (b) *X-ray photography of flange section taken after 4460 cycles*

Figure 19. *Damage progression in skin/stringer debond specimen 7B-06.*

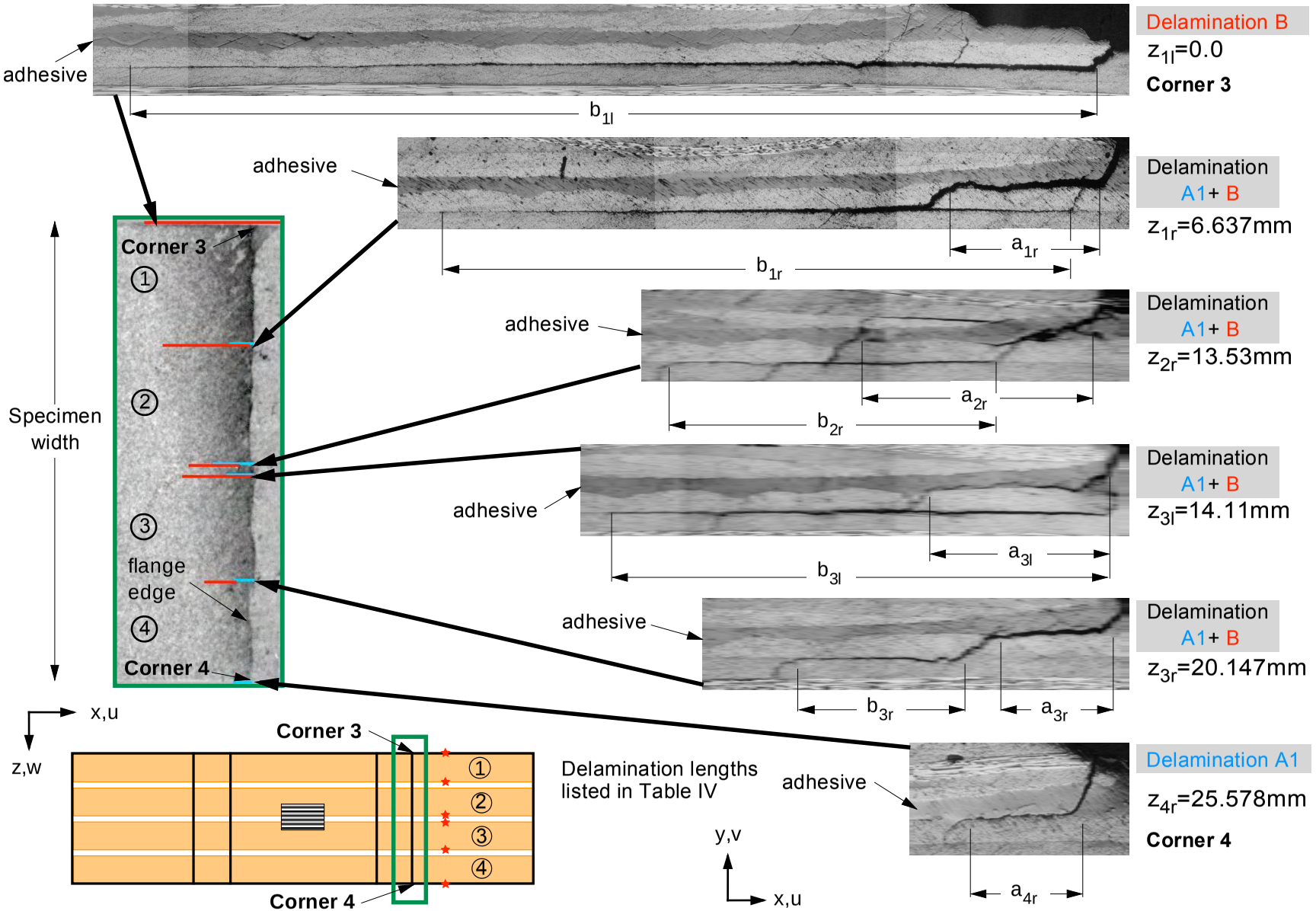

Figure 20. *Micrographs of interior sections along flange edge from corners 3 to 4 (specimen 8B-06).*

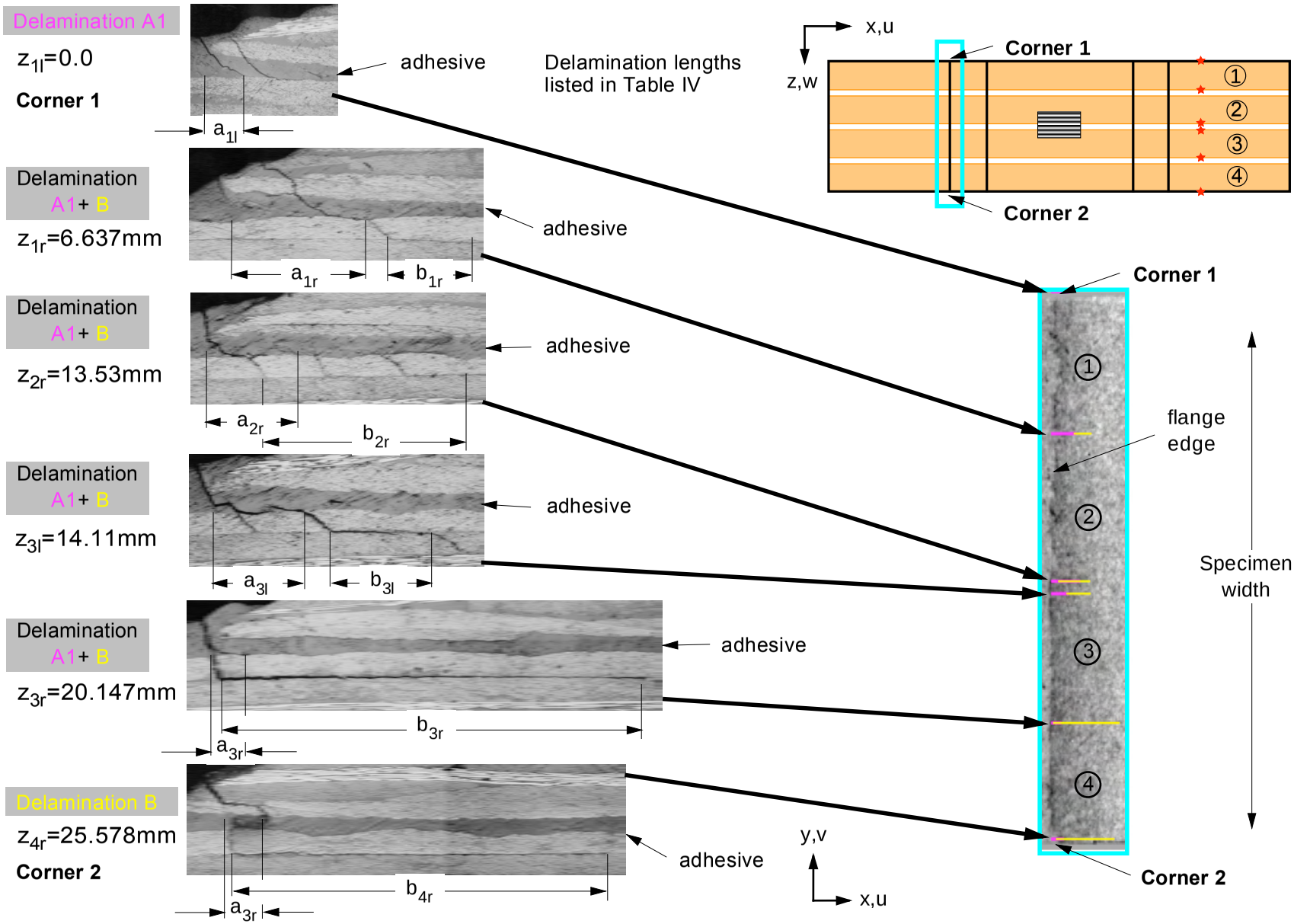

Figure 21. *Micrographs of interior sections along flange edge from corners 1 to 2 (specimen 8B-06).*

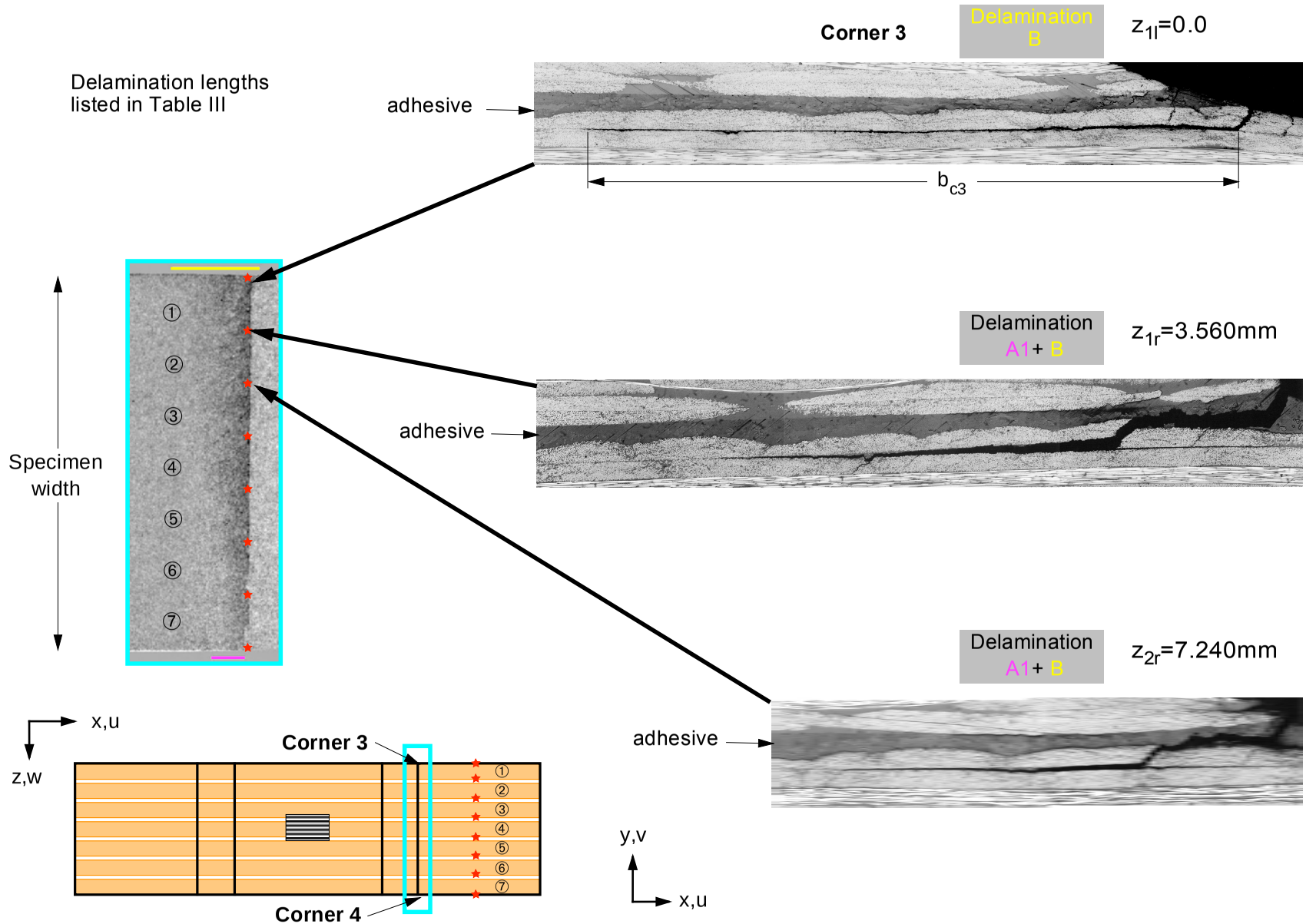

Figure 22a. *Micrographs of interior sections along flange edge from corners 3 to 4 (specimen 10B-03).*

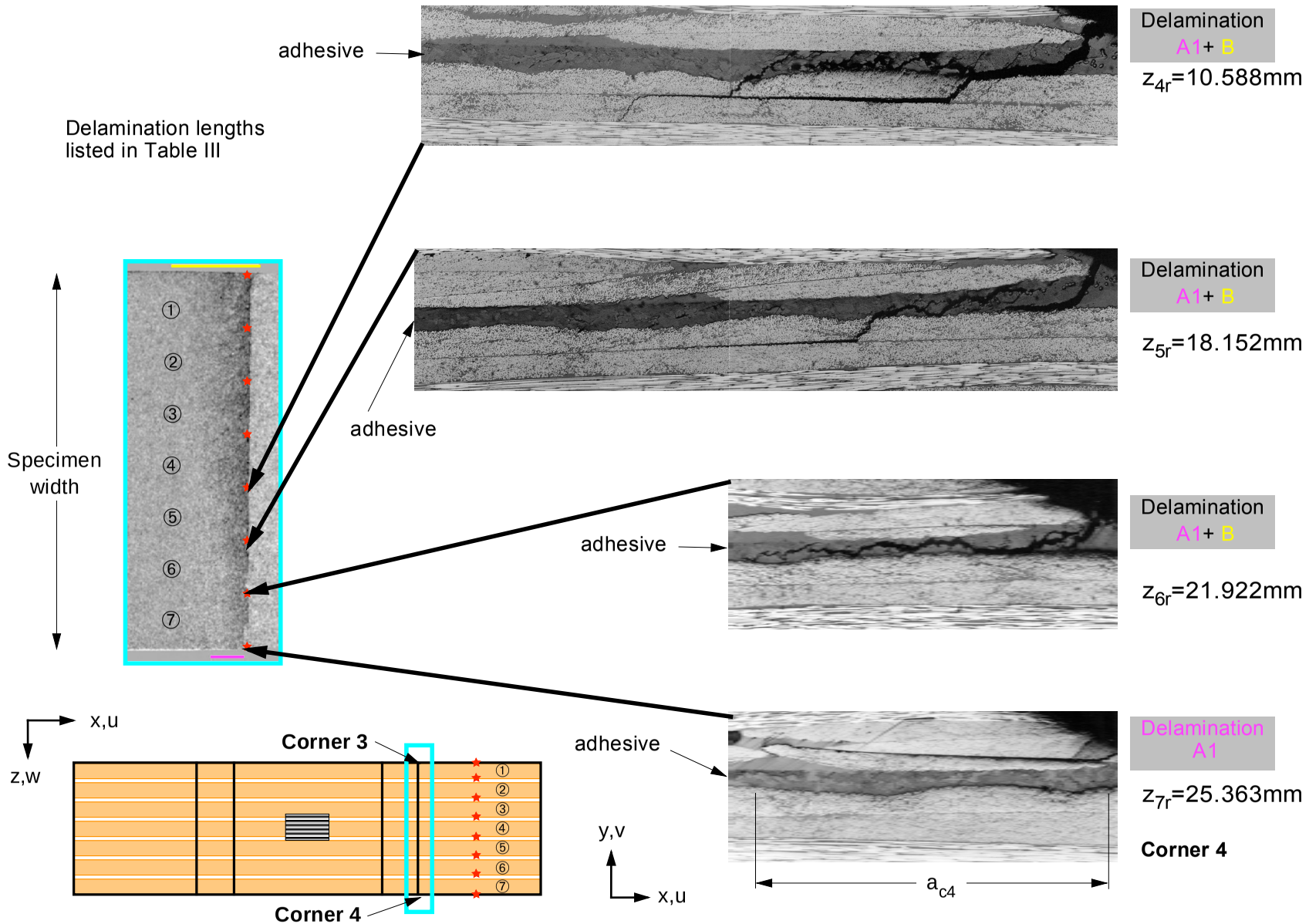

Figure 22b. *Micrographs of interior sections along flange edge from corners 3 to 4 (specimen 10B-03).*

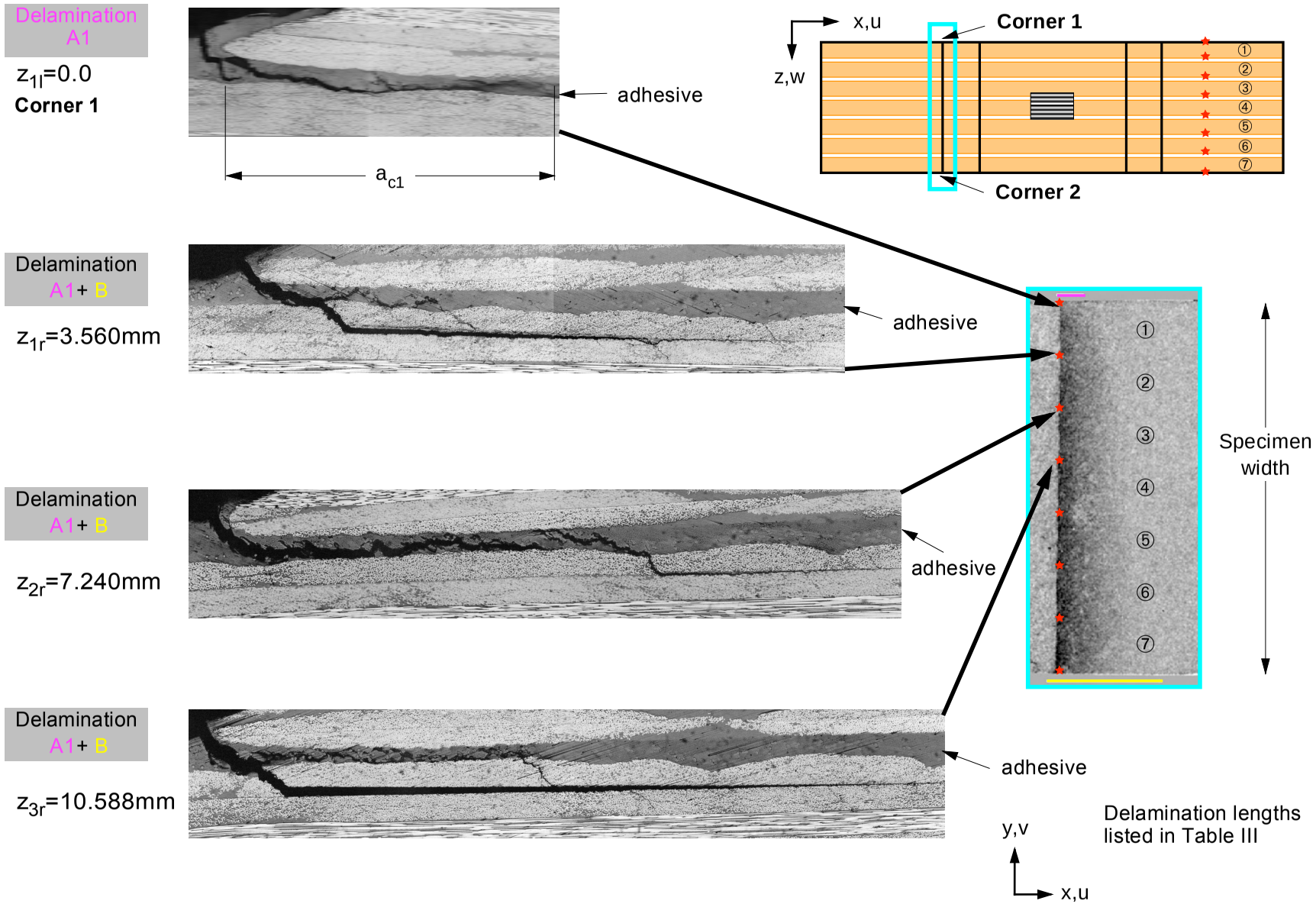

Figure 23a. *Micrographs of interior sections along flange edge from corners 1 to 2 (specimen 10B-03).*

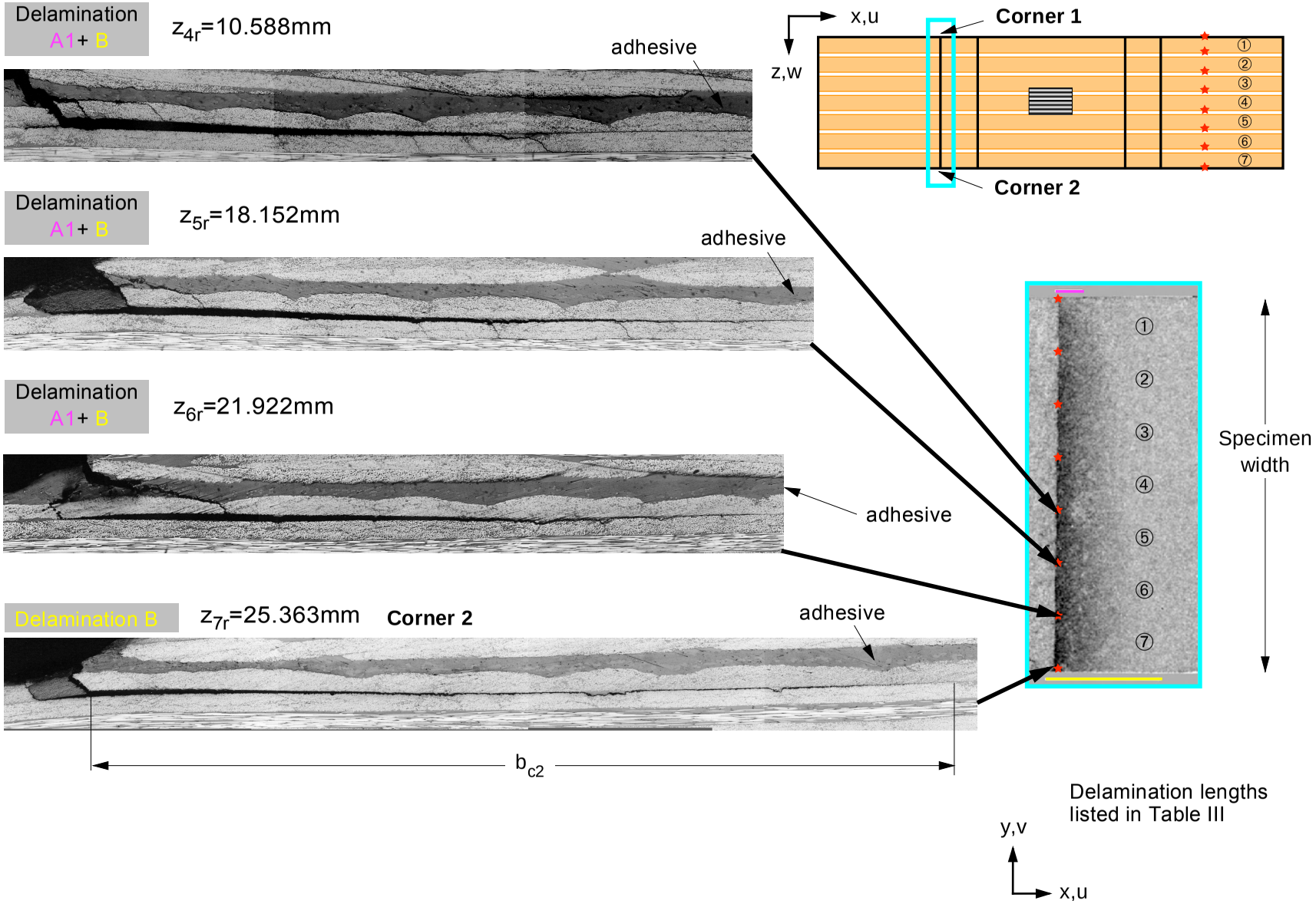

Figure 23b. *Micrographs of interior sections along flange edge from corners 1 to 2 (specimen 10B-03).*

REPORT DOCUMENTATION PAGE

Form Approved
OMB No. 0704-0188

1. REPORT DATE *(DD-MM-YYYY)*	2. REPORT TYPE	3. DATES COVERED *(From - To)*
01- 05 - 2008	Technical Memorandum	

4. TITLE AND SUBTITLE

Characterization of Fatigue Damage for Bonded Composite Skin/Stringer Configurations

5a. CONTRACT NUMBER

5b. GRANT NUMBER

5c. PROGRAM ELEMENT NUMBER

6. AUTHOR(S)

Paris, Isabelle; Cvitkovich, Michael; and Krueger, Ronald

5d. PROJECT NUMBER

5e. TASK NUMBER

5f. WORK UNIT NUMBER

698259.02.07.07.03.03

7. PERFORMING ORGANIZATION NAME(S) AND ADDRESS(ES)

NASA Langley Research Center
Hampton, VA 23681-2199

8. PERFORMING ORGANIZATION REPORT NUMBER

L-19468

9. SPONSORING/MONITORING AGENCY NAME(S) AND ADDRESS(ES)

National Aeronautics and Space Administration
Washington, DC 20546-0001

10. SPONSOR/MONITOR'S ACRONYM(S)

NASA

11. SPONSOR/MONITOR'S REPORT NUMBER(S)

NASA/TM-2008-215308

12. DISTRIBUTION/AVAILABILITY STATEMENT

Unclassified - Unlimited
Subject Category 24
Availability: NASA CASI (301) 621-0390

13. SUPPLEMENTARY NOTES

Work performed while Paris and Cvitkovich were NRC resident research associates at NASA Langley Research Center. Current affiliation: Paris, Composites Innovations, Inc., Monteal, Canada; Cvitkovich, Daimler AG, Wörth, Germany.
An electronic version can be found at http://ntrs.nasa.gov

14. ABSTRACT

The fatigue damage was characterized in specimens which consisted of a tapered composite flange bonded onto a composite skin. Quasi-static tension tests were performed first to determine the failure load. Subsequently, tension fatigue tests were performed at 40%, 50%, 60% and 70% of the failure load to evaluate the debonding mechanisms. For four specimens, the cycling loading was stopped at intervals. Photographs of the polished specimen edges were taken under a light microscope to document the damage. At two diagonally opposite corners of the flange, a delamination appeared to initiate at the flange tip from a matrix crack in the top 45° skin ply and propagated at the top 45°/-45° skin ply interface. At the other two diagonally opposite corners, a delamination running in the bondline initiated from a matrix crack in the adhesive pocket. In addition, two specimens were cut longitudinally into several sections. Micrographs revealed a more complex pattern inside the specimen where the two delamination patterns observed at the edges are present simultaneously across most of the width of the specimen. The observations suggest that a more sophisticated nondestructive evaluation technique is required to capture the complex damage pattern of matrix cracking and multi-level delaminations.

15. SUBJECT TERMS

Composites; Delamination propagation; Fatigue testing

16. SECURITY CLASSIFICATION OF:			17. LIMITATION OF ABSTRACT	18. NUMBER OF PAGES	19a. NAME OF RESPONSIBLE PERSON
a. REPORT	b. ABSTRACT	c. THIS PAGE			STI Help Desk (email: help@sti.nasa.gov)
					19b. TELEPHONE NUMBER *(Include area code)*
U	U	U	UU	40	(301) 621-0390